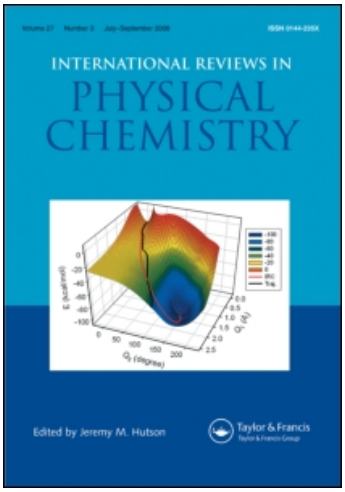

International Reviews in Physical Chemistry
Publication details, including instructions for authors and subscription information:
http://www.informaworld.com/smpp/title~content=t713724383

Non-linear optical spectroscopy as a novel probe for molecular chirality

M. A. Belkin[ab]; Y. R. Shen[ab]
[a] Department of Physics, University of California, Berkeley, CA 94720 [b] Lawrence Berkeley National Laboratory, Materials Sciences Division, Berkeley, CA 94720

To cite this Article Belkin, M. A. and Shen, Y. R.(2005) 'Non-linear optical spectroscopy as a novel probe for molecular chirality', International Reviews in Physical Chemistry, 24: 2, 257 — 299
To link to this Article: DOI: 10.1080/01442350500270601
URL: http://dx.doi.org/10.1080/01442350500270601

International Reviews in Physical Chemistry,
Vol. 24, No. 2, April–June 2005, 257–299

Taylor & Francis
Taylor & Francis Group

Non-linear optical spectroscopy as a novel probe for molecular chirality

M. A. BELKIN*† and Y. R. SHEN‡

Department of Physics, University of California, Berkeley, CA 94720 and
Materials Sciences Division, Lawrence Berkeley National Laboratory, Berkeley, CA 94720

(*Received 13 December 2004*)

Optical second-harmonic generation and sum-frequency generation as novel spectroscopic tools to probe molecular chirality are currently being developed. The latter in particular allows studies of chirality associated with both electronic and vibrational transitions of molecules in isotropic bulk, thin films, and monolayers. We review here the recent theoretical and experimental progress in the field. It is shown theoretically and experimentally that both processes can have monolayer sensitivity to detect chirality in electronic and vibrational transitions and that the sensitivity of the sum-frequency spectroscopy of chirality in vibrational transitions can be greatly enhanced through vibrational-electronic double-resonance. Measurements with short-pulsed lasers provide opportunities for time-resolved *in situ* studies of chirality.

Contents

*Corresponding author. Email: mbelkin@deas.harvard.edu
†Present address: Division of Engineering and Applied Sciences, Havard University, Cambridge, MA 02138.
‡Email: shenyr@socrates.berkeley.edu

International Reviews in Physical Chemistry
ISSN 0144–235X print/ISSN 1366–591X online
http://www.tandf.co.uk/journals
DOI: 10.1080/01442350500270601

1. Introduction

Chiral molecules are molecules not superposable with their mirror images by rotation and translation. Chirality (from the Greek word $\chi\epsilon\iota\rho$ – *cheir*, meaning hand) is a term first introduced by Lord Kelvin [1], and is intrinsically a three-dimensional notion. Being the basis of all life forms, chiral molecules play a very important role in modern chemistry, biology and medicine [2]. Most biological molecules in the human body consist of only left-handed amino-acids and right-handed sugars. The reason for that is still not fully understood. Chiral receptor sites in the body interact differently with molecules of different chirality and stereochemistry. This can result in marked differences in the pharmacological activities of enantiomers (see, e.g, [3]).

Traditional optical techniques used to probe molecular chirality are circular dichroism (CD) and Raman optical activity (ROA) [4]. They measure the differences in absorption coefficients (in CD) or scattering cross-sections (in ROA) of the chiral sample for left and right circularly polarized light. CD and ROA are not only capable of distinguishing left and right enantiomers, but are also very sensitive to molecular stereochemistry. Being purely optical techniques, CD and ROA have the intrinsic capability for non-destructive *in situ* measurements. However, the sensitivities of CD and ROA to molecular chirality are still limited. The reason is that the chiral optical responses of a chiral sample in CD and ROA come about only if one goes beyond the electric-dipole approximation and considers magnetic-dipole and electric-quadrupole transition moments in the analysis [4]. As a result, the CD of a chiral sample is only about 10^{-2}–10^{-3} of the absorption coefficient for electronic transitions and about 10^{-3}–10^{-4} for vibrational transitions [5, 6]. For ROA, the difference in scattered intensities of left and right circularly polarized laser light is typically $\sim 10^{-3}$–10^{-5} of the total scattered intensity [5, 7]. Thus CD and ROA are not sensitive enough to reliably detect chirality of a monolayer or thin film of molecules. This makes *in situ* probing of molecular chirality of biological systems difficult.

Optical second-harmonic generation (SHG) and sum-frequency generation (SFG) are electric-dipole allowed in media without inversion symmetry. This is the case for chiral media [8, 9]. It was predicted as early as in 1965 by Giordmaine that SFG should be observable in chiral liquids since molecular chirality generates non-vanishing elements in the non-linear susceptibility tensor of the sample. These elements are directly related to the chiral molecular structure and are of different signs for left and right enantiomers. Because the non-linear chiral responses are electric-dipole allowed, they could be as strong as the achiral responses. Knowing that achiral SHG and SFG can have a monolayer sensitivity, one would expect the same for chiral SHG and SFG, i.e. a much higher chiral sensitivity than CD and ROA.

Observation of SFG in chiral liquids was first reported by Rentzepis *et al.* in 1966 [10], but later attempts to reproduce their results were not successful [11, 12]. Hicks and coworkers in 1993 [13] first demonstrated the possibility of using SHG to probe molecular chirality and record the chiral electronic spectrum of a monolayer. Later, in our laboratory, we succeeded in using SFG spectroscopy to probe molecular chirality in vibrational transitions [14, 15] and electronic transitions [12, 16] in both surface monolayers and bulk liquids. Other groups, notably the groups of Koroteev, Persoons, Buckingham, and Albrecht, have also studied SHG and SFG from liquids,

monolayers, and thin films. In this paper, we review the optically active SHG and SFG processes in chiral media with an emphasis on the recent development of SFG spectroscopy to probe molecular chirality.

We note in passing that other chiral non-linear optical processes have also been investigated. Laser-induced optical activity and circular dichroism in chiral liquids have been reported by several groups [17–19]. They can be considered as third-order or four-wave mixing processes. The chiral response in all even-wave mixing experiments from isotropic or cubic chiral media is forbidden under the electric-dipole approximation [9]. Therefore, the induced optical activity and circular dichroism are necessarily weaker than their linear counterparts. However, potentially, they can be useful for studies of time-resolved chiral responses [19]. A chiral signal from five-wave mixing in a chiral liquid has also been reported [20]. Five-wave mixing spectroscopy has been proposed as a novel spectroscopic technique (dubbed as BioCARS) to study vibrational spectra of chiral biomolecules in solutions, in a way similar to Coherent Anti-Stokes Raman Spectroscopy (CARS) by Koroteev [21]. However, BioCARS has not yet been confirmed by others. Overall, there are very few experimental reports on the use of four- and five-wave mixing to probe molecular chirality.

2. Basics of chiral responses in SFG and SHG

2.1. *General considerations of SFG and SHG*

In recent years SHG and SFG have been well developed as spectroscopic techniques to study surfaces and interfaces. The basic principles of SHG and SFG and their applications can be found in recent review articles (see, for example, [22]; SHG is a degenerate case of SFG when both input beams have the same frequency). Here, for convenience of later discussions, we reproduce the essential aspects of the underlying theory for the processes with emphasis on the manifestation of chirality in SFG.

SFG is a second-order non-linear optical process arising from non-linear polarization at frequency $\omega_s = \omega_1 + \omega_2$ induced in a medium by two input fields $\vec{E}_1$ and $\vec{E}_2$ of frequencies ω_1 and ω_2 and wavevectors $\vec{k}_1$ and $\vec{k}_2$, respectively. The non-linear polarization including electric-quadrupole and magnetic-dipole contributions [23, 24] can be written as

$$\vec{P}^{(2)}_{\text{eff}}(\omega_s) = \vec{P}^{(2)}(\omega_s) - \vec{\nabla}\cdot\overleftrightarrow{Q}^{(2)}(\omega_s) + \frac{i}{\omega_s}\vec{\nabla}\times\vec{M}^{(2)}(\omega_s) \equiv \epsilon_0\overleftrightarrow{\chi}^{(2)} : \vec{E}_1\vec{E}_2, \tag{1}$$

where $\vec{P}^{(2)}$, $\overleftrightarrow{Q}^{(2)}$, and $\vec{M}^{(2)}$ are the non-linear electric-dipole polarization, electric-quadrupole polarization, and dipole magnetization, respectively, taking the form

$$\begin{aligned}\vec{P}^{(2)}(\omega_s) = {} & \epsilon_0\overleftrightarrow{\chi}^{(2)}_{\text{eee}} : \vec{E}_1\vec{E}_2 + \epsilon_0\overleftrightarrow{\chi}^{(2)}_{\text{eqe}} \vdots \vec{\nabla}\vec{E}_1\vec{E}_2 + \epsilon_0\overleftrightarrow{\chi}^{(2)}_{\text{eeq}} \vdots \vec{E}_1\vec{\nabla}\vec{E}_2 \\ & + \epsilon_0\overleftrightarrow{\chi}^{(2)}_{\text{eme}} : \left(\frac{\vec{\nabla}}{i\omega_1}\times\vec{E}_1\right)\vec{E}_2 + \epsilon_0\overleftrightarrow{\chi}^{(2)}_{\text{eem}} : \vec{E}_1\left(\frac{\vec{\nabla}}{i\omega_2}\times\vec{E}_2\right),\end{aligned}$$

$$\vec{\vec{Q}}^{(2)}(\omega_s) = \epsilon_0 \vec{\vec{\chi}}^{(2)}_{\mathrm{qee}} : \vec{E}_1 \vec{E}_2,$$
$$\vec{M}^{(2)}(\omega_s) = \epsilon_0 \vec{\vec{\chi}}^{(2)}_{\mathrm{mee}} : \vec{E}_1 \vec{E}_2. \tag{2}$$

Here, $\vec{\vec{\chi}}^{(2)}$ is the total second-order non-linear susceptibility tensor of the media, and $\vec{\vec{\chi}}^{(2)}_{\mathrm{abc}}$ denotes a component non-linear susceptibility tensor with the three subindices referring to either electric-dipole (e), or electric-quadrupole (q), or magnetic-dipole (m) contributions from the fields at ω_s, ω_1, and ω_2, respectively. We have neglected higher-order contributions from $\vec{\vec{\chi}}^{(2)}_{\mathrm{eqq}}$, $\vec{\vec{\chi}}^{(2)}_{\mathrm{emm}}$, $\vec{\vec{\chi}}^{(2)}_{\mathrm{qme}}$, etc. From equations (1) and (2), we obtain [25]:

$$\chi^{(2)}_{ijk} = \left(\chi^{(2)}_{\mathrm{eee}}\right)_{ijk} + \left(\chi^{(2)}_{Q1}\right)_{ijkl} k_{1l} + \left(\chi^{(2)}_{Q2}\right)_{ijkl} k_{2l} + \left(\chi^{(2)}_{Q}\right)_{ijkl} (k_{1l} + k_{2l}), \tag{3}$$
$$\left(\chi^{(2)}_{Q1}\right)_{ijkl} = i\left(\chi^{(2)}_{\mathrm{eqe}}\right)_{iljk} + \frac{1}{\omega_1}\left(\chi^{(2)}_{\mathrm{eme}}\right)_{ink} e_{nlj},$$
$$\left(\chi^{(2)}_{Q2}\right)_{ijkl} = i\left(\chi^{(2)}_{\mathrm{eeq}}\right)_{ijlk} + \frac{1}{\omega_2}\left(\chi^{(2)}_{\mathrm{eem}}\right)_{ijn} e_{nlk},$$
$$\left(\chi^{(2)}_{Q}\right)_{ijkl} = -i\left(\chi^{(2)}_{\mathrm{qee}}\right)_{lijk} - \frac{1}{\omega_s} e_{iln}\left(\chi^{(2)}_{\mathrm{mee}}\right)_{njk},$$

where e_{kln} is the Levi-Civita symbol and the lth Cartesian components of the wavevectors $\vec{k}_i$ are denoted as k_{il}. Note that the susceptibility tensors representing the electric-quadrupole and magnetic-dipole contributions are fourth-rank tensors. In many cases of SFG, the pure electric-dipole contribution from $\vec{\vec{\chi}}^{(2)}_{\mathrm{eee}}$ dominates; we then have $\vec{P}^{(2)}_{\mathrm{eff}}(\omega_s) \approx \vec{P}^{(2)}(\omega_s)$ and $\chi^{(2)}_{ijk} \approx (\chi^{(2)}_{\mathrm{eee}})_{ijk}$.

In the literature, the value of the non-linear susceptibility for a system depends on units and conventions. We will use SI units and adopt the convention following the field definition

$$\vec{E}(\vec{r}, t) = \vec{E} e^{-i(\omega t - \vec{k}\vec{r})} + \text{c.c.} \tag{4}$$

with $\vec{\vec{\chi}}^{(2)}$ for SFG being twice as large as for SHG as ω_1 approaches ω_2 [26].

Under the plane-wave approximation, the intensity of the sum-frequency (SF) output from a semi-infinite non-linear medium can be written as

$$I(\omega_s) = \frac{\omega_s^2}{8\epsilon_0 c^3 \cos^2(\beta_s)} |\chi^{(2)}_{\mathrm{eff}}|^2 I(\omega_1) I(\omega_2), \tag{5}$$

where $I(\omega_i)$ is the beam intensity at ω_i, β_s is the exit angle of the SF beam in air (see figure 1 for the experimental geometry) determined by matching of the input and output wavevector components parallel to the surface, and $\chi^{(2)}_{\mathrm{eff}}$ is the effective second-order non-linear susceptibility of the non-linear medium defined by

$$\chi^{(2)}_{\mathrm{eff}} = [\vec{\vec{L}}(\omega_s) \cdot \hat{e}_s] \cdot \left(\vec{\vec{\chi}}^{(2)}_S + \vec{\vec{\chi}}^{(2)}_B / (i\Delta k_z)\right) : [\vec{\vec{L}}(\omega_1) \cdot \hat{e}_1][\vec{\vec{L}}(\omega_2) \cdot \hat{e}_2]. \tag{6}$$

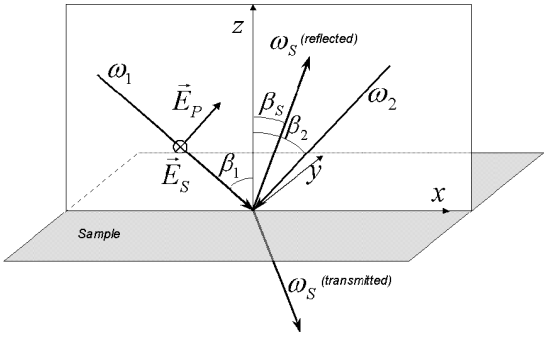

Figure 1. Beam geometry at sample position for a typical SFG experiment.

In equation (6), $\hat{e}_i$ is the unit polarization vector and $\overleftrightarrow{L}(\omega_i)$ the tensorial transmission Fresnel factor [22, 27] for the field at ω_i, $\Delta k_z \equiv (k_s)_z - (k_1)_z - (k_2)_z$ is the wavevector mismatch in the direction $\hat{z}$ along the surface normal, and $\overleftrightarrow{\chi}_S^{(2)}$ and $\overleftrightarrow{\chi}_B^{(2)}$ denote the non-linear susceptibilities of the surface and bulk, respectively, each assuming the general expression of equation (3). In general, both $\overleftrightarrow{\chi}_S^{(2)}$ and $\overleftrightarrow{\chi}_B^{(2)}$ can contribute to SFG. However, if $\overleftrightarrow{\chi}_B^{(2)}$ is electric-dipole allowed (in so-called non-linearly active media), the contribution from $\overleftrightarrow{\chi}_S^{(2)}$ is usually negligible. On the other hand, if $\overleftrightarrow{\chi}_B^{(2)}$ is electric-dipole forbidden while $\overleftrightarrow{\chi}_S^{(2)}$ is electric-dipole allowed, the two $\overleftrightarrow{\chi}^{(2)}$ terms in equation (6) can become comparable. In many cases when the surface molecular layer is well ordered and the bulk highly disordered, $\overleftrightarrow{\chi}_S^{(2)}$ can actually dominate over $\overleftrightarrow{\chi}_B^{(2)}$ and then SFG becomes surface-specific. This is particularly true for SFG in reflection where the wavevector mismatch $|\Delta k_z|$ is much larger than for SFG in transmission.

Depending on the structural symmetry of the medium, many of the tensor elements of the non-linear susceptibility tensors could vanish or depend on one another. In the next subsection, we shall describe the non-zero chiral and achiral elements of non-linear susceptibilities for azimuthally isotropic chiral surfaces and isotropic chiral bulks. They have been the two most common systems probed by chiral SHG and SFG.

2.2. *Non-linear susceptibility for an azimuthally isotropic chiral surface*

Because of the broken inversion symmetry, the surface non-linear susceptibility $\overleftrightarrow{\chi}_S^{(2)}$ is electric-dipole allowed, i.e. $\overleftrightarrow{\chi}_S^{(2)}$ is dominated by $(\overleftrightarrow{\chi}_{\mathrm{eee}}^{(2)})_S$. For an azimuthally isotropic surface in the laboratory coordinate system described in figure 1, the non-zero achiral elements of $\overleftrightarrow{\chi}_S^{(2)}$ are

$$\begin{aligned}
\left(\chi_S^{(2)}\right)_{xxz} &= \left(\chi_S^{(2)}\right)_{yyz}, \\
\left(\chi_S^{(2)}\right)_{xzx} &= \left(\chi_S^{(2)}\right)_{yzy}, \\
\left(\chi_S^{(2)}\right)_{zxx} &= \left(\chi_S^{(2)}\right)_{zyy}, \\
\left(\chi_S^{(2)}\right)_{zzz}&,
\end{aligned} \tag{7}$$

and the non-zero chiral elements are

$$\begin{aligned}\left(\chi_S^{(2)}\right)_{xyz} &= -\left(\chi_S^{(2)}\right)_{yxz},\\ \left(\chi_S^{(2)}\right)_{yzx} &= -\left(\chi_S^{(2)}\right)_{xzy},\\ \left(\chi_S^{(2)}\right)_{zxy} &= -\left(\chi_S^{(2)}\right)_{zyx}.\end{aligned} \tag{8}$$

For the chiral elements, the three-dimensional characteristics of chirality require the three subindices of $\overleftrightarrow{\chi}_S^{(2)}$ to be all different in this case. A mirror reflection from a plane perpendicular to the surface transforms a surface of right-hand (R) enantiomers to that of left-hand (S) enantiomers, and therefore changes the sign of the chiral elements. The chiral elements vanish for racemic mixtures or achiral surfaces.

With equation (6), one can see that experimentally the χ-elements in equation (7) can be assessed by SFG measurements with SSP (denoting S-, S- and P-polarization of the SF output at ω_s, the input at ω_1, and the input at ω_2, respectively), SPS, PSS, and PPP polarization combinations. The chiral elements can be assessed by SFG measurements with SPP, PSP, and PPS polarization combinations.

The surface non-linear susceptibility $\overleftrightarrow{\chi}_S^{(2)}$ is related to the hyperpolarizability $\overleftrightarrow{\alpha}^{(2)}$ [28] of the constituent molecules,

$$(\chi_S^{(2)})_{ijk} = \frac{1}{\epsilon_0} N_S l_S^{ii}(\omega_s) l_S^{jj}(\omega_1) l_S^{kk}(\omega_2) \sum_{\xi,\eta,\zeta} \alpha_{\xi\eta\zeta}^{(2)} \langle (\hat{i}\cdot\hat{\xi})(\hat{j}\cdot\hat{\eta})(\hat{k}\cdot\hat{\zeta})\rangle. \tag{9}$$

Here N_S is the number density of molecules on the surface, (i,j,k) and (ξ,η,ζ) refer the laboratory and molecular coordinates, respectively, $\overleftrightarrow{l}_S(\omega_i)$ is a tensor describing the microscopic local-field correction at ω_i [29], and $\langle\cdots\rangle$ denotes an average over the molecular orientational distribution. Traditional achiral SHG and SFG are often used to deduce information about molecular orientation if the relationship between $\overleftrightarrow{\alpha}^{(2)}$ and the molecular structure is known (see, e.g. [29, 30]). The chiral elements of $\overleftrightarrow{\chi}_S^{(2)}$ obtained from chiral SHG and SFG spectroscopy arise from molecular chirality, and hopefully can yield information on molecular chiral stereochemistry.

2.3. *Non-linear susceptibility for isotropic chiral bulk*

For a chiral isotropic bulk, the achiral elements of $\overleftrightarrow{\chi}_{\mathrm{eee}}^{(2)}$ vanish by symmetry and the only non-zero element of $\overleftrightarrow{\chi}_{\mathrm{eee}}^{(2)}$ is

$$\begin{aligned}\left(\chi_{\mathrm{eee}}^{(2)}\right)_{xyz} &= -\left(\chi_{\mathrm{eee}}^{(2)}\right)_{yxz} = \left(\chi_{\mathrm{eee}}^{(2)}\right)_{yzx}\\ &= -\left(\chi_{\mathrm{eee}}^{(2)}\right)_{zyx} = \left(\chi_{\mathrm{eee}}^{(2)}\right)_{zxy} = -\left(\chi_{\mathrm{eee}}^{(2)}\right)_{xzy} \equiv \chi_{\mathrm{chiral}}^{\mathrm{bulk}}.\end{aligned} \tag{10}$$

The lowest-order contribution to achiral $\overleftrightarrow{\chi}^{(2)}$ comes from $\overleftrightarrow{\chi}^{(2)}_{Q1}$, $\overleftrightarrow{\chi}^{(2)}_{Q2}$, and $\overleftrightarrow{\chi}^{(2)}_{Q}$ in equation (3). The non-zero elements of each of them are

$$\begin{aligned}
&\left(\chi^{(2)}_q\right)_{iijj} \equiv \chi_{q,1}, \quad \left(\chi^{(2)}_q\right)_{ijij} \equiv \chi_{q,2}, \quad \left(\chi^{(2)}_q\right)_{ijji} \equiv \chi_{q,3}, \\
&\left(\chi^{(2)}_q\right)_{iiii} = \chi_{q,1} + \chi_{q,2} + \chi_{q,3}.
\end{aligned} \tag{11}$$

where $q = Q1$, $Q2$, or Q, and $i,j = x$, y, or z. Under a mirror reflection that converts R-enantiomers to S-enantiomers or vice versa, $\overleftrightarrow{\chi}^{(2)}_{\text{eee}}$ changes sign, but $\overleftrightarrow{\chi}^{(2)}_{Q1}$, $\overleftrightarrow{\chi}^{(2)}_{Q2}$, and $\overleftrightarrow{\chi}^{(2)}_{Q}$ do not, as it should be. Again, the chiral elements of bulk $\overleftrightarrow{\chi}^{(2)}$ can be assessed by SPP, PSP and PPS polarization combinations, and the achiral elements by SSP, SPS, PSS and PPP polarization combinations (see equations (3) and (6)).

The chiral elements of $\overleftrightarrow{\chi}^{(2)}_{\text{eee}}$ are related to the chiral molecular hyperpolarizability $\overleftrightarrow{\alpha}^{(2)}$ by an isotropic averaging of the latter that yields

$$\chi^{\text{bulk}}_{\text{chiral}} = \frac{1}{\epsilon_0} N_B l_B(\omega_s) l_B(\omega_1) l_B(\omega_2) \cdot \alpha_{\text{chiral}}, \tag{12}$$

with

$$\alpha_{\text{chiral}} \equiv \sum_{\xi,\eta,\zeta} \alpha^{(2)}_{\xi\eta\zeta} \langle (\hat{x}\cdot\hat{\xi})(\hat{y}\cdot\hat{\eta})(\hat{z}\cdot\hat{\zeta})\rangle_{\text{iso}} = \frac{1}{6}\sum_{\xi,\eta,\zeta} \alpha^{(2)}_{\xi\eta\zeta} \cdot e_{\xi\eta\zeta}. \tag{13}$$

Here N_B is the number density of molecules in the bulk, $\langle\cdots\rangle_{\text{iso}}$ denotes the isotropic average in the bulk, $e_{\xi\eta\zeta}$ is the Levi-Civita symbol, and $l_B(\omega_i)$ is the local-field correction factor at ω_i for an isotropic bulk [31].

2.4. *Normalization of non-linear susceptibility*

To quantify the values of the measured non-linear susceptibility elements in SFG or SHG, we find it convenient to normalize the SFG or SHG output from a sample with that from a z-cut quartz crystal (α-SiO_2). Quartz is transparent in the range of 0.15–4 μm (50% transmission through a 1 mm thick sample) [32]. Its bulk structure has no inversion centre and produces an easily detectable SFG signal.

Crystalline quartz has D_3 [32] symmetry. If we choose the crystalline axes to coincide with the laboratory $(\hat{x},\hat{y},\hat{z})$ shown in figure 1, the non-vanishing elements of $\overleftrightarrow{\chi}^{(2)}_B$ of a z-cut quartz crystal are

$$\begin{aligned}
&\left(\chi^{(2)}_B\right)_{xxx} = -\left(\chi^{(2)}_B\right)_{xyy} = -\left(\chi^{(2)}_B\right)_{yyx} = -\left(\chi^{(2)}_B\right)_{yxy} \equiv \chi^{(2)}_q, \\
&\left(\chi^{(2)}_B\right)_{xyz} = -\left(\chi^{(2)}_B\right)_{yxz}, \\
&\left(\chi^{(2)}_B\right)_{xzy} = -\left(\chi^{(2)}_B\right)_{yzx}, \\
&\left(\chi^{(2)}_B\right)_{zxy} = -\left(\chi^{(2)}_B\right)_{zyx}.
\end{aligned} \tag{14}$$

but $\chi_q^{(2)}$ is much larger than the others. We generally normalize our measured SHG or SFG from a sample against that reflected from z-cut quartz using a SSP or PPP polarization combination to which only $\chi_q^{(2)}$ contributes. We assume

$$\chi_q^{(2)} = 4d_{11} = 1.60 \times 10^{-12}\,\mathrm{m\,V^{-1}} \tag{15}$$

with negligible dispersion, where $d_{11} = 0.40 \times 10^{-12}\,\mathrm{m\,V^{-1}}$ was obtained earlier by SHG with input at 1064 nm [33].

When an input, or output, or both beams have their frequencies near resonances, $\overleftrightarrow{\chi}_S^{(2)}$ and $\overleftrightarrow{\chi}_B^{(2)}$ are resonantly enhanced. Scanning ω_1, ω_2, or both over resonances yields a corresponding spectrum of the sample. We shall describe in the following sections SHG and SFG spectroscopic measurements that probe chirality in electronic and vibrational transitions of chiral molecules on surfaces or in isotropic bulks.

3. Second-harmonic generation from chiral media

SHG is a special case of SFG with $\omega_1 = \omega_2$. In this case, for an isotropic bulk, even the chiral elements of $\overleftrightarrow{\chi}_{\mathrm{eee}}^{(2)}$ should vanish because the input frequency degeneracy requires $(\chi_B^{(2)})_{ijk} = (\chi_B^{(2)})_{ikj}$, and yet as chiral elements, $(\chi_B^{(2)})_{ijk} = -(\chi_B^{(2)})_{ikj}$. However, both chiral and achiral SHG from an azimuthally isotropic chiral surface are still electric-dipole allowed. From equations (7) and (8), the non-zero elements of $\overleftrightarrow{\chi}_S^{(2)}$ for SHG are

$$\begin{aligned}
&\left(\chi_S^{(2)}\right)_{zzz} \equiv \chi_1\\
&\left(\chi_S^{(2)}\right)_{zxx} = \left(\chi_S^{(2)}\right)_{zyy} \equiv \chi_2\\
&\left(\chi_S^{(2)}\right)_{xxz} = \left(\chi_S^{(2)}\right)_{yyz} = \left(\chi_S^{(2)}\right)_{xzx} = \left(\chi_S^{(2)}\right)_{yzy} \equiv \chi_3\\
&\left(\chi_S^{(2)}\right)_{xyz} = -\left(\chi_S^{(2)}\right)_{yxz} = \left(\chi_S^{(2)}\right)_{yzx} = -\left(\chi_S^{(2)}\right)_{xzy} \equiv \chi_4.
\end{aligned} \tag{16}$$

The first three groups of elements in equation (16) are achiral and the last group is chiral. Because of degeneracy $\omega_1 = \omega_2$, the chiral elements $(\chi_S^{(2)})_{zxy} = -(\chi_S^{(2)})_{zyx}$ in equation (8) must vanish for SHG. Experimentally, the P-in/S-out polarization combination in SHG allows one to selectively probe the chiral elements. Other polarization combinations can also be used to assess the chiral elements through data analysis.

The first paper reporting successful application of SHG to probe molecular chirality of a surface monolayer was published by Hicks and coworkers in 1993 [13]. They observed that SHG spectra of electronic transitions of 1,1′-bi-2-naphthol (BN, $C_{20}H_{14}O_2$) adsorbed at air/water and air/fused quartz interfaces were different for left and right circularly polarized (CP) input beams. The difference was comparable to the average SHG intensity. Thus, the circular dichroic effect in SHG (SHG-CD), defined by Hicks as $2(I^- - I^+)/(I^- + I^+)$, with I^-, I^+ being the SHG intensity for left

and right CP inputs, was of the order of 1, or 10^2–10^3 times greater than that observed in a typical linear CD experiment. To appreciate this important characteristic of SHG-CD, we describe below their work in more detail.

Consider the case of a circularly polarized fundamental beam incident at 45° on a chiral surface with $\hat{z}$ being the surface normal and $\hat{y}$ perpendicular to the plane of incidence. The polarization of the beam is then described by

$$\hat{e}_1 = \hat{e}_2 = \frac{1}{2}\hat{x} + \frac{1}{2}\hat{z} \pm i\frac{1}{\sqrt{2}}\hat{y}, \tag{17}$$

where $\pm$ refers to right and left circularly polarized light, respectively. For a S or P polarized SHG signal in reflection, we obtain from equations (5), (6), and (16), neglecting the Fresnel factors,

$$\begin{aligned} I_S^{\pm}(2\omega) &\propto \left|\sqrt{2}\chi_3 \pm i\chi_4\right|^2 \\ I_P^{\pm}(2\omega) &\propto \left|\frac{1}{2}\chi_1 - \frac{1}{2}\chi_2 - \chi_3 \pm i\sqrt{2}\chi_4)\right|^2. \end{aligned} \tag{18}$$

Since χ_4, which reflects the chirality and is of opposite signs for R and S enantiomers, is electric-dipole allowed, it can be comparable to the achiral elements, χ_1, χ_2, and χ_3, and therefore, $2(I^- - I^+)/(I^- + I^+)$ or SHG-CD can be of order of one for both S and P polarizations. Figure 2 shows the SHG spectra from monolayers of R-BN and S-BN on water near their first electronic resonance obtained by Hicks and coworkers [13]. They were obtained with S-polarized second-harmonic (SH) output and left and right circularly polarized inputs. The measured value of SHG-CD at SHG wavelength ~290 nm was close to 1 [13].

As we mentioned earlier, we can use a P-in/S-out polarization combination to directly assess the surface chirality. In this case, the SH signal, seen from

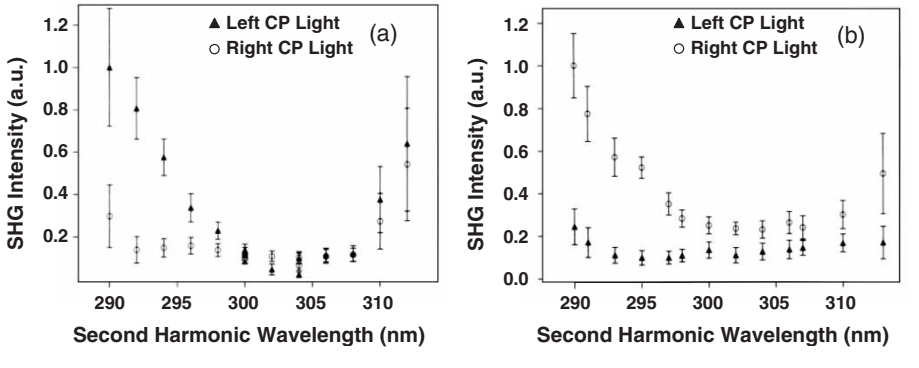

Figure 2. Spectral dependence of the S-polarized SHG signal from monolayers of R-BN (a) and S-BN (b) on a water surface for left and right CP fundamental, reprinted with permission from [13]. Copyright (1993), American Chemical Society.

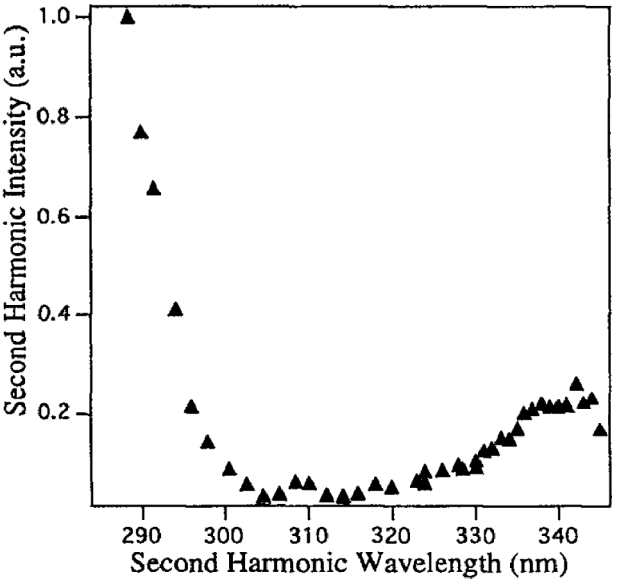

Figure 3. Spectral dependence of the S-polarized SHG signal from a monolayer of R-BN on water surface for P-polarized fundamental, reprinted with permission from [34]. Copyright (1994), American Institute of Physics.

equations (5), (6), and (16), is proportional to $|\chi_4|^2$. The P-in/S-out SHG spectrum of a monolayer of R-BN on water is shown in figure 3 [34]. (Further discussion of SF electronic spectra of BN will appear in the next section.) It is, however, the same for the two enantiomers. To distinguish R and S, one needs to have mixed contributions from both chiral and achiral elements of $\vec{\vec{\chi}}^{(2)}_S$ as in the case with circularly polarized inputs described by equation (18) [13, 35], or with inputs of linear polarizations, rotated by $\pm 45^\circ$ from the P (or S) polarization [36].

To show that chiral SHG can be an effective tool for biological systems, Hicks and coworkers used it to probe the chirality of poly-L-lysine adsorbed on fused silica [37] and cytochrome C (a membrane-associated protein) on interfaces in different environments [38, 39]. In the latter work, they found that the SHG-CD response is strongly affected by the oxidation state of the heme inside Cytochrome C.

Persoons and coworkers also studied SHG from chiral surfaces and thin films in some detail. To explain their data, they concluded that in addition to the electric-dipole contribution, they must include a significant proportion of magnetic-dipole contribution, $(\vec{\vec{\chi}}^{(2)}_{\text{mee}})_S$ and $(\vec{\vec{\chi}}^{(2)}_{\text{eem}})_S$ $(= (\vec{\vec{\chi}}^{(2)}_{\text{eme}})_S)$, in the surface non-linear susceptibility [40–43]. This is surprising because it is well known that the magnetic-dipole (and also electric-quadrupole) contribution to $(\vec{\vec{\chi}}^{(2)})_S$ is often two to three orders of magnitude smaller than the electric-dipole contribution in the optical range. The difficulty could arise from the sensitivity of the experimental data to the experimental geometry and the uniqueness of the data-fitting procedure involving many (20) adjustable parameters [43, 44]. Hache and coworkers used a similar analysis on their SHG study of a chiral surface [45]. They assumed both input and output frequencies are off-resonance and

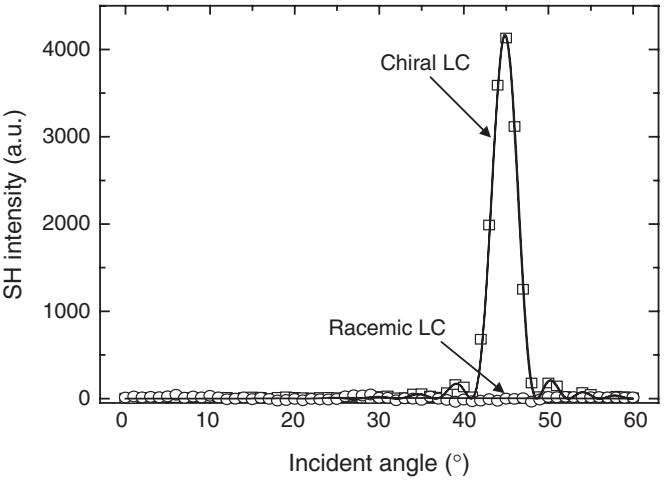

Figure 4. SHG from a homeotropically aligned film of W314 as a function of the incident angle around phase matching. The solid curve is the theoretical fit. Reprinted with permission from [55]. Copyright (2004) by the Optical Society of America.

found that the largest components of $(\overleftrightarrow{\chi}^{(2)}_{\mathrm{mee}})_S$ and $(\overleftrightarrow{\chi}^{(2)}_{\mathrm{eem}})_S$ are only about 3% of the largest components of $(\overleftrightarrow{\chi}^{(2)}_{\mathrm{eee}})_S$, but for the chiral elements the magnitudes of $(\overleftrightarrow{\chi}^{(2)}_{\mathrm{eee}})_S$, $(\overleftrightarrow{\chi}^{(2)}_{\mathrm{mee}})_S$, and $(\overleftrightarrow{\chi}^{(2)}_{\mathrm{eem}})_S$ appeared to be comparable. This seems to indicate that the chiral components of $(\overleftrightarrow{\chi}^{(2)}_{\mathrm{eee}})_S$ are much smaller than the achiral ones. More investigation with frequency variation toward resonance and emphasis on microscopic understanding of the origin of molecular chirality will help solve the mystery.

Frey and coworkers [46], Conboy and coworkers [47, 48], and others [49–54] have also used chiral SHG to study surfaces and thin films of chiral molecules. In particular, Conboy and coworkers demonstrated that the intrinsic chirality of proteins probed by SHG can be used to monitor their association to a surface [47]. A detailed summary of SHG measurements of chiral surfaces and thin polymer films can be found in a recent review by Persoons *et al.* [41].

As discussed earlier, SHG is not electric-dipole allowed in isotropic chiral liquids even though chiral liquids have no inversion symmetry. This is no longer the case if the chiral liquids are anisotropic because the symmetry of the medium is now similar to that of an oriented chiral molecular monolayer with non-zero chiral χ-elements given by equations (16). We have demonstrated such a case using a homeotropically aligned chiral smectic-A liquid crystal (LC) sample (W314) [55]. The anisotropy also allows the achievement of phase matching of SHG in the bulk by angle tuning (see figure 4), which strongly enhances the signal. The chiral SHG dropped precipitously as the sample underwent the transition from the smectic-A to the isotropic phase as it should (see figure 5).

4. Chiral sum-frequency spectroscopy of electronic transitions

It seems natural to extend SHG studies of chirality to SFG. With independently tunable visible and infrared sources, SFG can be used to probe electronic and vibrational

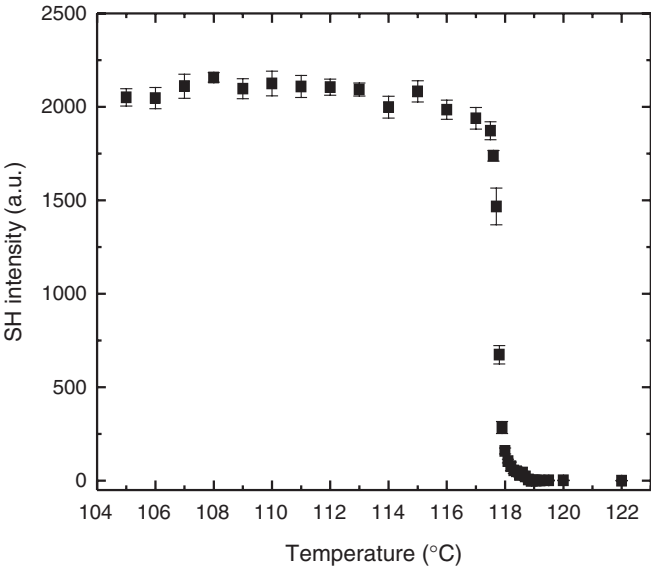

Figure 5. Temperature dependence of phase matched SHG from W314. The smectic-A to isotropic phase transition occurred at 117.6°C. Reprinted with permission from [55]. Copyright (2004) by the Optical Society of America.

transitions [22] with more flexibility, and therefore is a much more powerful analytical tool than SHG. Like SHG, SFG is electric-dipole allowed at an azimuthally isotropic surface, but unlike SHG, SFG is also electric-dipole allowed by symmetry in an isotropic chiral bulk, as first suggested by Giordmaine in 1965 [8]. Rentzepis *et al*. did report the observation of chiral SFG in arabinose solution in 1966 [10], but their results have never been confirmed [11]. We believe the reason is that both input and output frequencies in their experiment were too far away from resonance. The resonant part of the microscopic expression for a second-order molecular polarizability is given by [28]:

$$\alpha_{ijk}^{(2)} = \frac{1}{\hbar^2}\sum_{n,n'}\left[\frac{\langle g|\mu_i|n\rangle\langle n|\mu_j|n'\rangle\langle n'|\mu_k|g\rangle}{(\omega_s-\omega_{ng}+i\Gamma_{ng})(\omega_2-\omega_{n'g}+i\Gamma_{n'g})} + \frac{\langle g|\mu_i|n\rangle\langle n'|\mu_j|g\rangle\langle n|\mu_k|n'\rangle}{(\omega_s-\omega_{ng}+i\Gamma_{ng})(\omega_1-\omega_{n'g}+i\Gamma_{n'g})}\right], \tag{19}$$

where $|n\rangle$ and $|n'\rangle$ denote the molecular energy states and we assumed, for simplicity, all molecules to be initially in the ground state $|g\rangle$. Following equation (19), we can show that α_{chiral}, defined in equation (13), takes the form

$$\alpha_{\text{chiral}} = \frac{1}{6\hbar^2}\sum_{n,n'}\left[\frac{\langle g|\vec{\mu}|n\rangle\cdot\langle n|\vec{\mu}|n'\rangle\times\langle n'|\vec{\mu}|g\rangle}{(\omega_s-\omega_{ng}+i\Gamma_{ng})(\omega_2-\omega_{n'g}+i\Gamma_{n'g})} + \frac{\langle g|\vec{\mu}|n\rangle\cdot\langle n'|\vec{\mu}|g\rangle\times\langle n|\vec{\mu}|n'\rangle}{(\omega_s-\omega_{ng}+i\Gamma_{ng})(\omega_1-\omega_{n'g}+i\Gamma_{n'g})}\right]. \tag{20}$$

If the input and output frequencies are far away from resonance such that the system can be approximated by an effective two-level system with an average resonant frequency $\overline{\omega}_{ng}$, we obtain from equation (20) that $\alpha_{\text{chiral}} \approx 0$. This agrees with the general result that no chirality can exist in a two-level system. Thus we expect that in order to observe chiral SFG, we must have either the input or the output frequency close to resonance. Therefore, we have studied chiral SFG near electronic resonances from a BN bulk solution, recalling that Hicks and coworkers already carried out SHG spectroscopy on BN monolayers.

We used SFG in transmission to probe the chiral response of a 0.7 M solution of BN in tetrahydrofuran (THF). To access the chiral components of the non-linear susceptibility, $(\chi_B^{(2)})_{ijk}$ with $i \neq j \neq k$, we must have the three input and output beam polarization vectors not in the same plane. More specifically, from equations (5), (6), and (10), we find the chiral SFG output in transmission to be

$$I(\omega_s) \propto \left| \chi_{\text{chiral}}^{\text{bulk}} \hat{e}_s \cdot (\hat{e}_1 \times \hat{e}_2) \frac{1}{\Delta k_z} \right|^2, \tag{21}$$

where $\hat{e}_i$ is the polarization of the ith beam. The coherence length, $l_c = 1/|\Delta k_z|$, is often maximized when the input and output beams are collinear, but then $\hat{e}_s \cdot (\hat{e}_1 \times \hat{e}_2)$ will be zero. To optimize the product of $|l_c|$ and $|\hat{e}_s \cdot (\hat{e}_1 \times \hat{e}_2)|$, one would choose the polarization combination SPP and a beam geometry with the angle between $\vec{k}_1$ and $\vec{k}_2$ to be $\sim$10–20°, depending on the values of the refractive indices of the sample for input and output beams. However, for such small angles, the coherence length is very sensitive to the values of the refractive indices, which are often not known precisely. This makes the analysis of the spectra difficult. In practice, unless the maximum sensitivity is needed, we found it more convenient to have the angle between $\vec{k}_1$ and $\vec{k}_2$ around 30–60°. The coherence length is then much less sensitive to the refractive indices while the chiral SFG signal is only $\sim$3 times smaller than that in the optimal case.

Our experimental arrangement is depicted schematically in figure 6(a). The input beams were generated from a picosecond laser/optical parametric system. One beam (ω_1), tunable from 450 to 550 nm with 250 μJ/pulse, was obliquely incident at 45°, and the other ω_2, fixed at 1.064 μm with 2 mJ/pulse, was normally incident on the sample. The sample was a cell of BN solution 2 mm thick. This cell thickness was much larger than the coherence length, but small enough so that the linear optical rotation in the solution is negligible. The two input beams were focused to a diameter of $\sim$1 mm and overlapped in time and space at the exit surface of the solution to avoid strong absorption of the SF output near resonance. The SF output from the sample, after passing through a filter assembly and a double monochromator, was detected and recorded by a photomultiplier/photon-counting system. Sum-frequency signals in both SPP and PSP polarization combinations yielded $|\chi_{\text{chiral}}^{\text{bulk}}|^2$ (see equations (5), (6), and (10)), although the signal strengths are different.

The linear absorption spectrum and the molecular structure of BN are shown in figure 7 and the observed chiral SF spectra of the BN solution covering the first pair of electronic transitions of BN in the range between 315 and 360 nm are presented in figure 8. The peak positions in linear and non-linear optical spectra agree well.

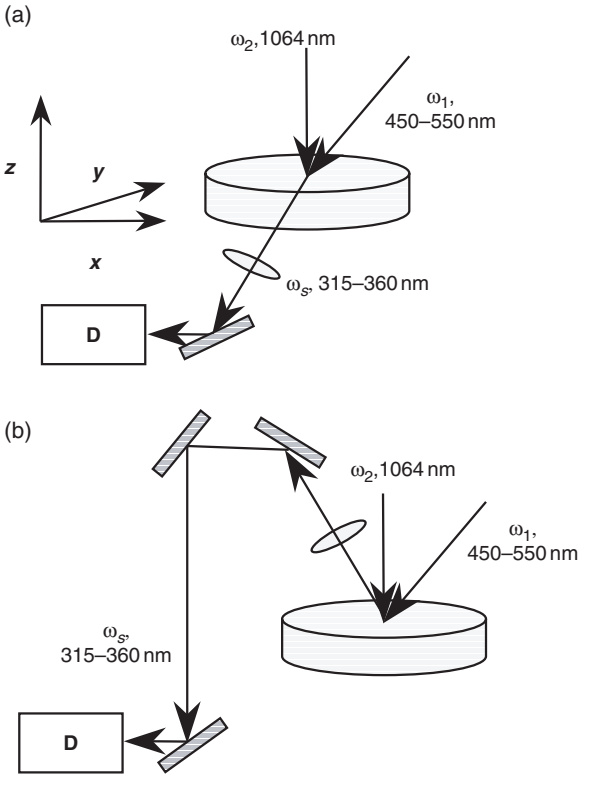

Figure 6. Experimental arrangement for (a) bulk measurements and (b) surface measurements (geometry 1).

The spectrum disappeared for a racemic mixture of BN solution as expected. We have also presented in figure 9 the deduced spectrum of $|\chi^{\text{bulk}}_{\text{chiral}}/N_B|^2$. As shown in the figure, the spectrum of $|\chi^{\text{bulk}}_{\text{chiral}}/N_B|^2$ can be fitted very well using equations (12) and (20), which with ω_s close to two resonances at $\omega_{e_{1_+}g}$ and $\omega_{e_{1_-}g}$ give

$$\frac{1}{N_B}\chi^{\text{bulk}}_{\text{chiral}} = \frac{1}{N_B}\left(\frac{A_B^+}{\omega_s - \omega_{e_{1_+}g} + i\Gamma_{e_{1_+}g}} + \frac{A_B^-}{\omega_s - \omega_{e_{1_-}g} + i\Gamma_{e_{1_-}g}}\right). \tag{22}$$

The values of A_B^+ (for transition at 319 nm) and A_B^- (for transition at 338 nm) obtained from the fitting are given in table 1.

We can relate the chiral response to the chiral structure of BN using the so-called coupled-oscillator model [56].[1] As shown in figure 7(a), the BN molecule is composed

[1] Note that some numerical factors and signs in equation (20), (28), (29), and (31) in this review article differ from those in equations (11), (12), (13), and (15), respectively, in the reference because of the arithmetic errors made in the reference. As a result, the values of $|\chi^{\text{bulk}}_{\text{chiral}}/N_B|$ shown in figure 10(b) are smaller than those shown in figure 2 in the reference by approximately a factor of 2. Because of the qualitative nature of the coupled-oscillator model, these errors have no affect on the general conclusions of the reference.

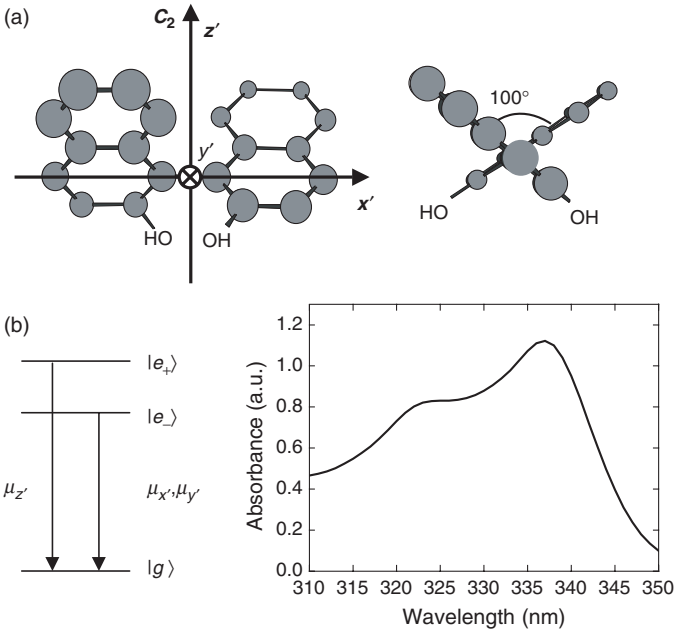

Figure 7. (a) Structure of the 1,1′-bi-2-naphthol molecule: front view (left) and side view (right) with molecular axes $\hat{x}'$, $\hat{y}'$, and $\hat{z}'$. (b) Transitions between the lowest exciton-split states and the ground state and the corresponding absorption spectrum of BN in tetrahydrofuran (that in acetone is similar). Reprinted with permission from [16]. Copyright (2002) by the American Physical Society.

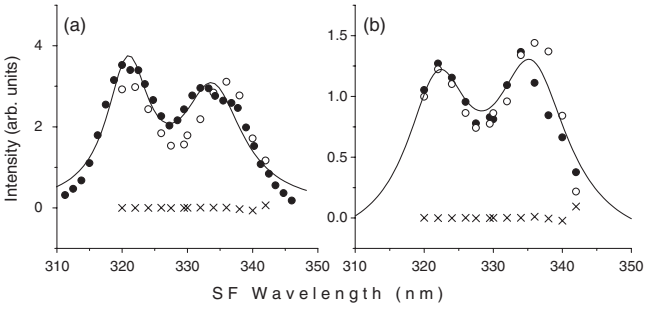

Figure 8. Transmission SFG spectra of BN in THF with (a) SPP and (b) PSP polarization combinations. Filled circles are for S-BN, open circles for R-BN, and crosses for the racemic mixture. Solid lines are to guide the eye. Reprinted with permission from [12] and [16]. Copyright (2001, 2002) by the American Physical Society.

of two linked 2-naphthol monomers, twisted by 100° [57]. The twist gives rise to chirality. The classical coupled-oscillator model, first proposed by Kuhn [58] to explain linear optical activity, treats each monomer as an oscillator. Hache *et al.* [59] recently used it to describe the second-order optical response from an azimuthally isotropic chiral monolayer. The quantum coupled-oscillator model treats the monomers quantum mechanically and is certainly more quantitative and realistic. It was also first developed to understand linear optical activity of dimer molecules [60, 61]. Here, we extend the

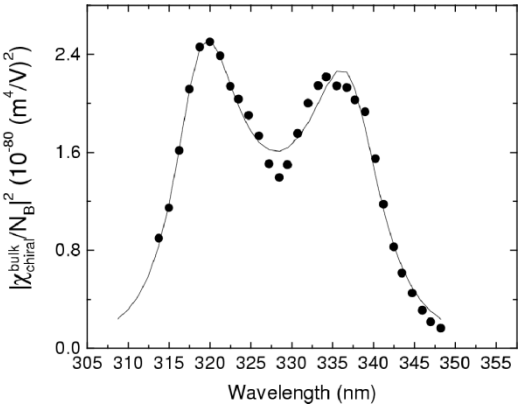

Figure 9. The spectrum of $|\chi^{bulk}_{chiral}/N_B|^2$ of a 0.7 M solution of S-BN in tetrahydrofuran. The solid curve is the fit from equation (22). Reprinted with permission from [16]. Copyright (2002) by the American Physical Society.

Table 1. Fitting parameters for χ^{bulk}_{chiral} of a 0.7 M solution of S-BN in tetrahydrofurane and $(\chi^{(2)}_S)_{ijk}$ of a monolayer of R-BN on water, as described in equation (22) and equation (39), respectively. Reprinted with permission from [16]. Copyright (2002) by the American Physical Society.

Bulk chiral elements	$\lvert A^{\pm}_B\rvert$ (m V^{-1} s^{-1})	λ_{ab} (nm)	$\Gamma_{ab}/2\pi c$ (cm^{-1})
$(\chi^{(2)}_B)_{xyz} = (\chi^{(2)}_B)_{yzx} = (\chi^{(2)}_B)_{zxy} =$	5.2	338	477
$-(\chi^{(2)}_B)_{yxz} = -(\chi^{(2)}_B)_{xzy} = -(\chi^{(2)}_B)_{zyx}$	6.5	319	479
Surface chiral elements	$\lvert(A^{\pm}_S)_{ijk}\rvert$ (m^2 V^{-1} s^{-1})	λ_{ab} (nm)	$\Gamma_{ab}/2\pi c$ (cm^{-1})
$(\chi^{(2)}_S)_{yxz} = -(\chi^{(2)}_S)_{xyz}$	1.0×10^{-7}	338	668
$(\chi^{(2)}_S)_{yzx} = -(\chi^{(2)}_S)_{xzy}$	1.0×10^{-7}	338	668
$(\chi^{(2)}_S)_{zxy} = -(\chi^{(2)}_S)_{zyx}$	0.4×10^{-7}}	321	664

calculation to the second-order non-linear polarizability of BN. The two identical monomers of BN, if not coupled, would lead to a pair of degenerate states for each excited monomer state. Coupling between the monomers lifts the degeneracy, resulting in a set of so-called exciton-split pairs of states, $|e_{n_+}\rangle$ and $|e_{n_-}\rangle$, that are respectively symmetric and antisymmetric with respect to a two-fold rotation about the molecular symmetry axis. Let $\hat{x}'$ be along the connecting C–C bond and $\hat{z}'$ along the C_2 symmetry axis of the molecule (figure 7(a)). Then a simple symmetry argument shows that the only non-vanishing electric-dipole matrix elements between $\langle e_{n_\pm}|$ and $|g\rangle$ are $\langle e_{n_+}|\mu_{z'}|g\rangle$ and $\langle e_{n_-}|\mu_i|g\rangle$ with $i = x'$ or y'. For the first pair of excited states $|e_{1_\pm}\rangle$, the transitions from $|g\rangle$ to $|e_{1_+}\rangle$ occur at 319 nm and from $|g\rangle$ to $|e_{1_-}\rangle$ at 338 nm [57].

We can now insert the exciton-split states in equation (20) and with equation (12) obtain the microscopic expressions for $A^{\pm}_B$ defined in equation (22)

$$A^{\pm}_B = \frac{1}{\epsilon_0} N_B l_B(\omega_s) l_B(\omega_1) l_B(\omega_2) A_{\pm}, \tag{23}$$

with

$$A_{\pm} = \frac{1}{6\hbar^2}(\omega_1 - \omega_2)\langle g|\vec{\mu}|e_{1_{\pm}}\rangle \cdot \sum_n \left[\frac{\langle e_{1_{\pm}}|\vec{\mu}|n\rangle \times \langle n|\vec{\mu}|g\rangle}{(\omega_1 - \omega_{ng})(\omega_2 - \omega_{ng})}\right], \tag{24}$$

where $|n\rangle$ denotes the energy states of the dimer.

More explicitly, in the coupled-oscillator model, the ground electronic state of the dimer is given by

$$|g\rangle = |0\rangle|0'\rangle, \tag{25}$$

where $|0\rangle$ and $|0'\rangle$ refer to the ground electronic states of the two monomers. The symmetric and antisymmetric excited electronic states have the expressions

$$|e_{n_{\pm}}\rangle = \frac{1}{\sqrt{2}}(|0\rangle|n'\rangle \pm |n\rangle|0'\rangle), \tag{26}$$

with $|n\rangle$ and $|n'\rangle$ denoting the first excited states of the two individual monomers. The energy difference between the symmetric and the antisymmetric state, known as the Davydov exciton splitting, is

$$E_{e_{n_+}} - E_{e_{n_-}} = 2\langle n|\langle 0'|V|0\rangle|n'\rangle, \tag{27}$$

with V being the interaction potential between the monomers. The electric-dipole operator for the dimer in equation (24) should now be replaced by the sum of the electric-dipole operators, $\vec{\mu}$ and $\vec{\mu}'$ for the monomers. We then find the more explicit expressions of $A_{\pm}$ in terms of the monomer states.

$$\begin{aligned} A_{\pm} = \pm\frac{(\omega_1 - \omega_2)}{24\hbar^2}\Bigg[&\frac{(\vec{\mu}_{01} + \vec{\mu}'_{01}) \cdot (\Delta\vec{\mu}_{10} - \Delta\vec{\mu}'_{10}) \times (\vec{\mu}_{10} - \vec{\mu}'_{10})}{(\omega_2 - \omega_{e_{1_{\mp}}g})(\omega_1 - \omega_{e_{1_{\mp}}g})} \\ &\pm \sum_{n\geq 2}(\vec{\mu}_{01} \pm \vec{\mu}'_{01}) \cdot \left(\frac{(\vec{\mu}_{1n} \pm \vec{\mu}'_{1n}) \times (\vec{\mu}_{n0} + \vec{\mu}'_{n0})}{(\omega_2 - \omega_{e_{n+}g})(\omega_1 - \omega_{e_{n+}g})} + \frac{(\vec{\mu}_{1n} \mp \vec{\mu}'_{1n}) \times (\vec{\mu}_{n0} - \vec{\mu}'_{n0})}{(\omega_2 - \omega_{e_{n-}g})(\omega_1 - \omega_{e_{n-}g})}\right)\Bigg], \end{aligned} \tag{28}$$

where $\vec{\mu}_{ab}$ and $\vec{\mu}'_{ab}$ denote the transition dipole moments of the two monomers between states $|a\rangle$ and $|b\rangle$, $\Delta\vec{\mu}_{10} \equiv \vec{\mu}_{11} - \vec{\mu}_{00}$, and $\Delta\vec{\mu}'_{10} \equiv \vec{\mu}'_{11} - \vec{\mu}'_{00}$.

If we neglect the difference between $\omega_{e_{n_+}g}$ and $\omega_{e_{n_-}g}$ in the above expression, and realize that $\vec{\mu}_{1i} \cdot (\vec{\mu}_{i0} \times \vec{\mu}'_{10}) = \vec{\mu}'_{1i} \cdot (\vec{\mu}'_{i0} \times \vec{\mu}_{10})$ from the C_2 symmetry of the dimer, we can simplify equation (28) to

$$\begin{aligned} A_{\pm} = \frac{(\omega_1 - \omega_2)}{24\hbar^2}\Bigg[&\pm\left\{\frac{4\Delta\vec{\mu}_{10} \cdot (\vec{\mu}_{10} \times \vec{\mu}'_{10})}{(\omega_2 - \omega_{e_1g})(\omega_1 - \omega_{e_1g})} + \sum_{n\geq 2}\frac{4\vec{\mu}_{1n} \cdot (\vec{\mu}_{n0} \times \vec{\mu}'_{10})}{(\omega_2 - \omega_{e_ng})(\omega_1 - \omega_{e_ng})}\right\} \\ &+ \sum_{n\geq 2}\frac{4\vec{\mu}_{1n} \cdot (\vec{\mu}_{n0} \times \vec{\mu}_{10})}{(\omega_2 - \omega_{e_ng})(\omega_1 - \omega_{e_ng})}\Bigg], \end{aligned} \tag{29}$$

with

$$\omega_{e_n g} \equiv \frac{\omega_{e_{n+}g} + \omega_{e_{n-}g}}{2}.$$

The last term describes chirality in the monomer components of the dimer molecule, and vanishes if they are achiral. The terms in the curly brackets describe the chirality of the dimer resulting from the twist between the monomers, and is non-zero even if the monomers are achiral. As a further simplification, we neglect the dispersion of the denominators in the summation in equation (29) and replace the transition frequencies $\omega_{e_n g}$ with $n \geq 2$ by an effective transition frequency ω_{eff}. This approximation transforms the system into an effective three-level system. We then find for BN, with the help of the closure relation of eigenstates,

$$\sum_{n\geq 2} \frac{4\vec{\mu}_{1n} \cdot (\vec{\mu}_{n0} \times \vec{\mu}'_{10})}{(\omega_2 - \omega_{e_n g})(\omega_1 - \omega_{e_n g})} \approx \frac{-4\Delta\vec{\mu}_{10} \cdot (\vec{\mu}_{10} \times \vec{\mu}'_{10})}{(\omega_2 - \omega_{\text{eff}})(\omega_1 - \omega_{\text{eff}})} \tag{30}$$

and hence,

$$\begin{aligned} A_{\pm} = \pm \frac{(\omega_1 - \omega_2)}{6\hbar^2} \Delta\vec{\mu}_{10} \cdot (\vec{\mu}_{10} \times \vec{\mu}'_{10}) \\ \times \left[\frac{1}{(\omega_2 - \omega_{e_1 g})(\omega_1 - \omega_{e_1 g})} - \frac{1}{(\omega_2 - \omega_{\text{eff}})(\omega_1 - \omega_{\text{eff}})} \right] \end{aligned} \tag{31}$$

We can now use equations (22), (23), and (31) to calculate $|\chi^{\text{bulk}}_{\text{chiral}}/N_B|$ versus ω_s for BN and compare the result with experiment. The two connected naphthalene subunits in BN are twisted by an angle $\alpha \sim 100^\circ$ [57]. From table 8-3 of [62], we find $|\Delta\vec{\mu}_{10}| = 0.5$ Debye and from [57], we find $|\vec{\mu}_{10}| = 1.4$ Debye with $\vec{\mu}_{10}$ lying in the monomer plane and making an angle of $\theta_1 = 40^\circ$ with the short axis of the monomer. The direction of $\Delta\vec{\mu}_{10}$ is not known; we assume that it lies in the ring plane and makes an angle of θ_0 with the long axis of the monomer. The geometry of BN in figure 10(a) gives

$$\Delta\vec{\mu}_{10} \cdot (\vec{\mu}_{10} \times \vec{\mu}'_{10}) = |\Delta\vec{\mu}_{10}||\vec{\mu}_{10}|^2 \cdot \sin(\alpha)\sin(\theta_1)\sin(\theta_1 - \theta_0). \tag{32}$$

For numerical estimates, we take $\theta_0 = 90^\circ$ and $\hbar\omega_{\text{eff}} = 6$ eV to roughly coincide with the position of the first strong absorption peak of BN. With ω_1 varied and ω_2 fixed at $\hbar\omega_2 = 1.17$ eV (wavelength at 1.064 μm), the calculated SF spectrum of $|\chi^{\text{bulk}}_{\text{chiral}}/N_B|$ versus ω_s is displayed in figure 10(b) in comparison with the experimental spectrum obtained from a 0.7 M solution of BN in tetrahydrofuran (THF). In the calculation, we used $\hbar\omega_{e_{1_+}g} = 3.89$ eV (or wavelength 319 nm), $\hbar\omega_{e_{1_-}g} = 3.67$ eV (or 338 nm), and $\Gamma_{e_{1_\pm}g} = 480\,\text{cm}^{-1}$ (see table 1). We utilized the Lorentz formula for local-field factors $l_B(\omega_i) = (\epsilon(\omega_i) + 2)/3$ with $\epsilon(\omega_i)$ being 1.46, 1.39, and 1.37 at ω_i equal to ω_s, ω_1 and ω_2, respectively. The agreement between theoretical and experimental spectra is very good considering the simplifying assumptions made in the calculation. The absolute

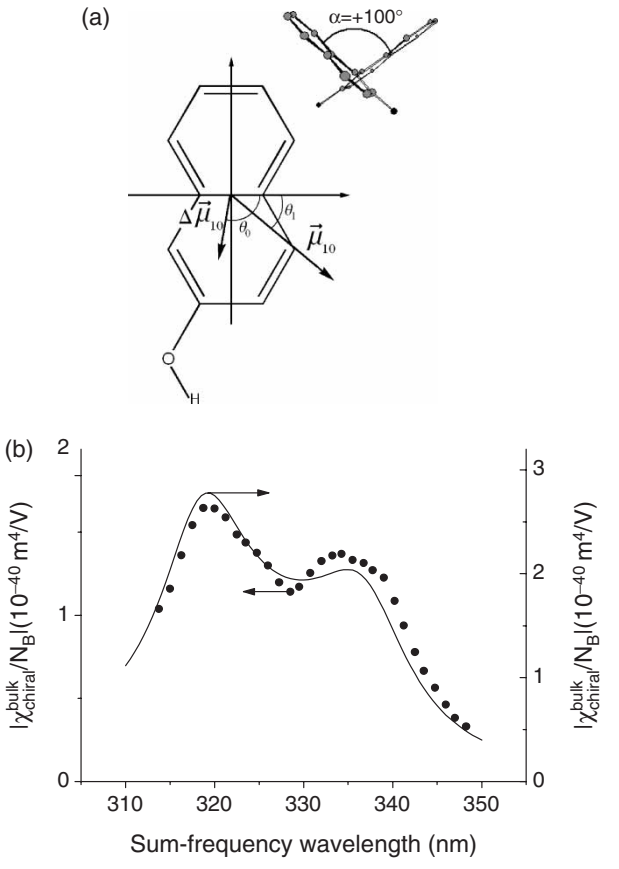

Figure 10. (a) Structure of the monomers of the BN molecule. (b) Experimental result (dots) and model prediction (solid line) of $|\chi^{bulk}_{chiral}/N_B|$ versus ω_s for a 0.7 M solution of S-BN in tetrahydrofuran.

value of $A_{\pm}$, for example, will reduce significantly if θ_0 is closer to 40° than 90°. While the value of θ_0 may be obtained from calculation, it could be deduced from fitting a doubly resonant SF spectrum with $\omega_1 \approx \omega_{e_{1-}g}$ and $\omega_s \approx \omega_{e_{1+}g}$. In this case, the terms with $n \geq 2$ in the expression of $A_{\pm}$ can be neglected, and the system becomes more truly a three-level system. More generally, the doubly resonant SFG spectrum can provide a more rigorous check of the theory discussed here.

Equation (32) shows how the chiral non-linearity depends on the structure of BN. In a three-level approximation, for non-vanishing χ^{bulk}_{chiral} the three vectors $\Delta\vec{\mu}_{10}$, $\vec{\mu}_{10}$ and $\vec{\mu}'_{10}$ must not be in the same plane: $\vec{\mu}_{10}$ and $\vec{\mu}'_{10}$ must not be along the short axis of the monomers and $\Delta\vec{\mu}_{10}$ must be tilted away from $\vec{\mu}_{10}$. The twist angle α has opposite signs for the two enantiomers, S-BN and R-BN.

It is interesting to know whether linear optical activity and chiral SFG at the same electronic resonances provide similar or different chiral structural information about chiral molecules. The linear optical activity arises from the difference of refractive indices, n_L and n_R, for left and right circularly polarized light, respectively. For a

chiral liquid we have [60, 61]

$$n_R - n_L = \frac{2}{3} c\mu_0 N l_B(\omega) \cdot \frac{2}{\hbar} \sum_{m \neq g} \frac{\omega \cdot R_{mg}}{(\omega - \omega_{mg} + i\Gamma_{mg})(\omega + \omega_{mg} - i\Gamma_{mg})}, \tag{33}$$

where $R_{mg} \equiv \mathrm{Im}(\vec{\mu}_{gm} \cdot \vec{m}_{mg})$, ω is the optical frequency, $l_B(\omega)$ is the local-field correction factor for the bulk, $\vec{\mu}$ and $\vec{m}$ are electric and magnetic dipole operators, respectively, and we have assumed that only the ground state is populated.

Using the coupled-oscillator model, we find for a dimer molecule like BN [60, 61]

$$R_{e_{n_\pm} g} = \pm \frac{1}{4} \omega_{e_{n_\pm} g} \vec{R} \cdot (\vec{\mu}'_{n0} \times \vec{\mu}_{n0}), \tag{34}$$

where $\vec{R}$ is the vector connecting the centres of the two monomers. With $\omega \sim \omega_{e_{1_\pm} g}$, we can write

$$\frac{n_R - n_L}{N} \approx \frac{B_+}{\omega - \omega_{e_{1_+} g} + i\Gamma_{e_{1_+} g}} + \frac{B_-}{\omega - \omega_{e_{1_-} g} + i\Gamma_{e_{1_-} g}}, \tag{35}$$

with

$$B_\pm = \pm \frac{1}{3\hbar} c\mu_0 l_B(\omega) \frac{\omega \omega_{e_1 g}}{\omega + \omega_{e_1 g}} \vec{R} \cdot (\vec{\mu}'_{10} \times \vec{\mu}_{10}). \tag{36}$$

The chiral structural information is contained in $B_\pm$ in linear optical activity as $A_\pm$ in chiral SFG. In both cases, if the two achiral monomers are not coupled so that $\omega_{e_{1_+} g} = \omega_{e_{1_-} g}$, or are not twisted with respect to each other so that $\vec{\mu}'_{10} \times \vec{\mu}_{10} = 0$, then the chiral response must vanish. However, the linear optical activity depends on the dot product of the $\vec{R}$ and $(\vec{\mu}'_{10} \times \vec{\mu}_{10})$, but the chiral SFG response depends on the dot product of $\Delta\vec{\mu}_{10}$ and $(\vec{\mu}_{10} \times \vec{\mu}'_{10})$ (in simplified form). The former means that the strength of optical activity actually increases with the physical separation of the two monomers, and the form $\vec{R} \cdot (\vec{\mu}'_{10} \times \vec{\mu}_{10})$ is a manifestation of the non-local, partially magnetic-dipole origin of the linear optical activity [4]. On the other hand, for chiral SFG, the chiral response is proportional to the vector product of three dipole moments and hence is a local response. Thus, linear optical activity and chiral SFG actually provide different information about the chiral structure of a dimer molecule.

The chiral SFG can be extended to cases involving double resonances in three levels. While resonant linear optical activity or circular dichroism probes chirality in selected electronic transition through $\vec{R} \cdot (\vec{\mu}'_{10} \times \vec{\mu}_{10})$, doubly resonant chiral SFG can probe chirality in transitions among the three selected levels through (following equation (20)) $\vec{\mu}_{gn} \cdot (\vec{\mu}_{nn'} \times \vec{\mu}'_{n'g})$. In general, double resonance can occur with one electronic and one vibrational transition. Therefore, one can anticipate more chiral structural information about a molecule from doubly resonant SFG.

It is clearly possible to extend SFG to the probing of chiral electronic resonances of BN monolayers as a similar SHG measurement was already reported by Hicks and coworkers [13, 34, 35]. However, SFG spectroscopy does have more flexibility in variations of beam geometry and polarization that can lead to more information. Because of selection rules, the SF spectra of an oriented monolayer are generally different from those of the bulk. Here, we discuss our chiral SFG work on BN monolayers on water.

The monolayer samples were prepared from a saturable solution of BN in water. The BN molecules would segregate to the air/water interface to form a more or less oriented monolayer with OH terminals facing toward the water. In the SFG measurement, the SF output was detected in the reflected direction. We focused on chiral SF spectroscopy over the first pair of electronic transitions of BN.

To measure the three independent chiral surface non-linear susceptibility elements in equation (8) for the BN monolayer on water, we used two different beam geometries. In geometry 1 (figure 6b), the ω_1 beam was incident at an angle of $\theta_1 = 45^\circ$ and the ω_2 beam at $\theta_2 = 0^\circ$. As seen from equations (5), (6), and (8), the SPP and PSP polarization combinations then allowed us to assess $(\chi_S^{(2)})_{yzx}$ and $(\chi_S^{(2)})_{zyx}$, respectively. The PPS combination yielded the linear combination of $(\chi_S^{(2)})_{zxy} = -(\chi_S^{(2)})_{zyx}$ and $(\chi_S^{(2)})_{xzy} = -(\chi_S^{(2)})_{yzx}$. In geometry 2, the ω_1 and ω_2 beams were incident on the surface at $\theta_1 = 45^\circ$ and $\theta_2 = 30^\circ$. The SPP polarization combination assessed the linear combination of $(\chi_S^{(2)})_{yzx}$ and $(\chi_S^{(2)})_{yxz}$. With $(\chi_S^{(2)})_{yzx}$ already known, $(\chi_S^{(2)})_{yxz}$ could be deduced. The measured values of the non-linear susceptibilities were normalized against signals from a reference quartz crystal.

The chiral spectra of the different geometries and polarization combinations for a BN monolayer on water are displayed in figure 11. The spectra of the two enantiomers of BN are the same while that of the racemic mixture vanishes as shown in figure 11(a) for the SPP spectra. This assures us that the spectra come from the non-linear chiral response. We notice in figure 11(a) and (b) that with both geometries, the SPP spectra exhibit only a single resonance peak at 338 nm for $\omega_s \sim \omega_{e_{1_-}g}$ and no resonant peak at 321 nm for $\omega_s \sim \omega_{e_{1_+}g}$. This is also the case for the P-in/S-out SHG spectrum of BN on water observed by Hicks, figure 3, suggesting that the BN monolayer is oriented.

To understand the surface SFG spectra, we consider first the non-linear polarizability elements of BN molecules. We obtain from equation (19), in the molecular coordinates,

$$\alpha^{(2)}_{i'j'z'} = \frac{1}{\hbar^2}\sum_n \left[\frac{\langle g|\mu_{i'}|e_{1_-}\rangle\langle e_{1_-}|\mu_{j'}|n\rangle\langle n|\mu_{z'}|g\rangle}{(\omega_s - \omega_{e_{1_-}g} + i\Gamma_{e_{1_-}g})(\omega_2 - \omega_{ng})} + \frac{\langle g|\mu_{i'}|e_{1_-}\rangle\langle e_{1_-}|\mu_{z'}|n\rangle\langle n|\mu_{j'}|g\rangle}{(\omega_s - \omega_{e_{1_-}g} + i\Gamma_{e_{1_-}g})(\omega_1 - \omega_{ng})}\right],$$

$$\alpha^{(2)}_{i'z'j'} = \frac{1}{\hbar^2}\sum_n \left[\frac{\langle g|\mu_{i'}|e_{1_-}\rangle\langle e_{1_-}|\mu_{z'}|n\rangle\langle n|\mu_{j'}|g\rangle}{(\omega_s - \omega_{e_{1_-}g} + i\Gamma_{e_{1_-}g})(\omega_2 - \omega_{ng})} + \frac{\langle g|\mu_{i'}|e_{1_-}\rangle\langle e_{1_-}|\mu_{j'}|n\rangle\langle n|\mu_{z'}|g\rangle}{(\omega_s - \omega_{e_{1_-}g} + i\Gamma_{e_{1_-}g})(\omega_1 - \omega_{ng})}\right],$$

$$\alpha^{(2)}_{z'i'j'} = \frac{1}{\hbar^2}\sum_n \left[\frac{\langle g|\mu_{z'}|e_{1_+}\rangle\langle e_{1_+}|\mu_{i'}|n\rangle\langle n|\mu_{j'}|g\rangle}{(\omega_s - \omega_{e_{1_+}g} + i\Gamma_{e_{1_+}g})(\omega_2 - \omega_{ng})} + \frac{\langle g|\mu_{z'}|e_{1_+}\rangle\langle e_{1_+}|\mu_{j'}|n\rangle\langle n|\mu_{i'}|g\rangle}{(\omega_s - \omega_{e_{1_+}g} + i\Gamma_{e_{1_+}g})(\omega_1 - \omega_{ng})}\right], \quad (37)$$

for $i', j' = x'$ or y', but $i' \neq j'$. We have neglected the damping constants in the off-resonant denominators. Since only $\langle e_{n_+}|\mu_{z'}|g\rangle$ and $\langle e_{n_-}|\mu_i|g\rangle$ with $i = x'$ or y' are

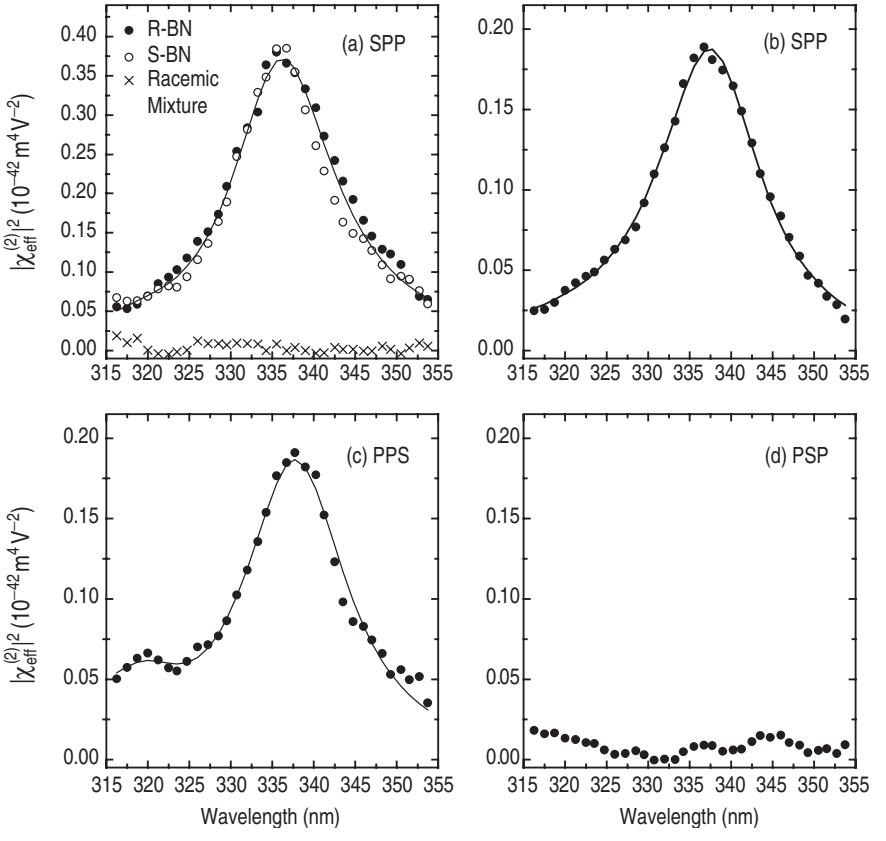

Figure 11. Chiral SFG spectra from surface monolayers of BN. (a) SPP spectra from monolayers of R-BN, S-BN and their racemic mixture measured with experimental geometry 2; (b) SPP (c) PPS and (d) PSP spectra from a monolayer of R-BN, measured with experimental geometry 1. Solid curves are fits from equation (39). Reprinted with permission from [16]. Copyright (2002) by the American Physical Society.

non-vanishing, $\alpha^{(2)}_{i'j'z'}$ and $\alpha^{(2)}_{i'z'j'}$ are resonantly enhanced only at $\omega_s = \omega_{e_1-g}$ and $\alpha^{(2)}_{z'i'j'}$ only at $\omega_s = \omega_{e_1+g}$. The observed spectra indicate that both $(\chi^{(2)}_S)_{yzx}$ and $(\chi^{(2)}_S)_{yxz}$ should not contain $\alpha^{(2)}_{z'x'y'}$ and $\alpha^{(2)}_{z'y'x'}$. For this to be true, the BN surface monolayer must have molecules well oriented with their molecular z'-axis along the surface normal (z). (Such an orientation is reasonable considering that the OH terminals of BN should adsorb on water and the aromatic rings are highly hydrophobic.) The corresponding surface chiral non-linear susceptibility elements are, from equation (9),

$$\left(\chi^{(2)}_S\right)_{yxz} = \frac{1}{\epsilon_0} N_S l^{yy}_S(\omega_s) l^{xx}_S(\omega_1) l^{zz}_S(\omega_2)\left(\alpha^{(2)}_{y'x'z'} - \alpha^{(2)}_{x'y'z'}\right)/2,$$
$$\left(\chi^{(2)}_S\right)_{xzy} = \frac{1}{\epsilon_0} N_S l^{xx}_S(\omega_s) l^{zz}_S(\omega_1) l^{yy}_S(\omega_2)\left(\alpha^{(2)}_{x'z'y'} - \alpha^{(2)}_{y'z'x'}\right)/2,$$
$$\left(\chi^{(2)}_S\right)_{zyx} = \frac{1}{\epsilon_0} N_S l^{zz}_S(\omega_s) l^{yy}_S(\omega_1) l^{xx}_S(\omega_2)\left(\alpha^{(2)}_{z'y'x'} - \alpha^{(2)}_{z'x'y'}\right)/2, \quad (38)$$

where $\overleftrightarrow{l}_S(\omega_i)$ is the local-field correction factor for the surface monolayer for the beam at ω_i (note that $l_S^{xx}(\omega_i) = l_S^{yy}(\omega_i)$). Thus, the SPP polarization combination assessing only $(\chi_S^{(2)})_{yzx}$ yields a single resonance at 338 nm, and the PPS spectrum assessing $(\chi_S^{(2)})_{xzy}$ and $(\chi_S^{(2)})_{zxy}$ exhibits resonances at both 321 and 338 nm. Because $|(\chi_S^{(2)})_{zxy}|$ is small (as it would vanish by symmetry if $\omega_1 = \omega_2$), the peak at 321 nm in the PPS spectrum is weak. Its visibility is partly due to constructive interference through overlap with the tail of the strong peak at 338 nm in the coherent SFG process. In contrast, the PSP spectrum, assessing only $(\chi_S^{(2)})_{zyx}$, shows only the resonance at $\omega_s \sim \omega_{e_{1_+}g}$, and then, without the benefit of constructive interference with the strong peak at 338 nm, the peak becomes too weak to detect as seen in figure 11(d). The surface non-linear susceptibility elements near resonance can be expressed in the general form

$$\left(\chi_S^{(2)}\right)_{ijk} = \frac{(A_S^+)_{ijk}}{\omega_s - \omega_{e_{1_+}g} + i\Gamma_{e_{1_+}g}} + \frac{(A_S^-)_{ijk}}{\omega_s - \omega_{e_{1-}g} + i\Gamma_{e_{1-}g}}, \tag{39}$$

which can be used to fit the spectra in figure 11. The parameters $(A_S^{\pm})_{ijk}$ and $\Gamma_{e_{1_\pm}g}$ deduced from the fitting are listed in table 1.

For comparison, we also measured the achiral spectral response from the BN monolayer using PPP, SSP, SPS and PSS polarization combinations. The PPP spectra are shown in figure 12 as an example. Here, the spectra for monolayers of R-BN, S-BN and a racemic mixture appear identical as expected. The resonance peak at 321 nm comes from $(\chi_S^{(2)})_{zzz}$ and $(\chi_S^{(2)})_{zxx}$ and the one at 338 nm from $(\chi_S^{(2)})_{xxz}$ and $(\chi_S^{(2)})_{xzx}$, as seen from equations (5), (6), (7), and (37). The comparable intensities of achiral and chiral spectra indicate that the chiral and achiral non-linear susceptibility elements are of the same order of magnitude.

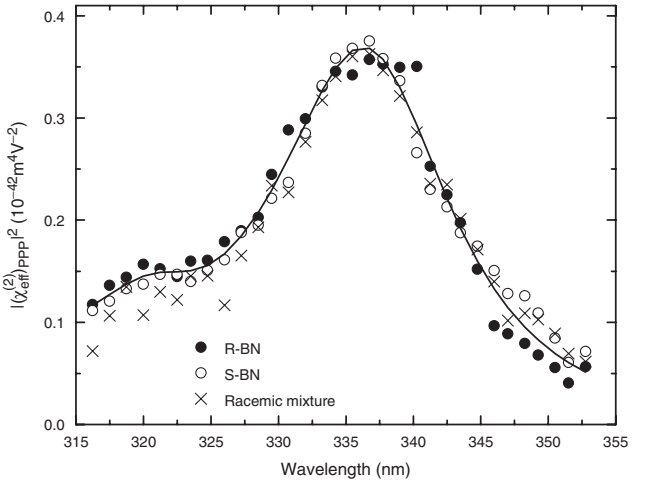

Figure 12. PPP spectra from surface monolayers of R-BN, S-BN, and their racemic mixture, measured with experimental geometry 2 (see the text). The solid curve is the fit from equation (39). Reprinted with permission from [16]. Copyright (2002) by the American Physical Society.

To see how ordered and disordered molecular orientations can affect the chiral SF response, we can compare $|A_B^{\pm}|/N_B$ with $|(A_S^{+})_{zyx}|/N_S$ and $|(A_S^{-})_{yzx}|/N_S$ at $\omega_s \sim \omega_{e_{1_+}g}$ and $\omega_s \sim \omega_{e_{1_-}g}$, respectively. We obtain

$$\frac{|(A_S^{+})_{zyx}|/N_S}{|A_B^{+}|/N_B} = 2.6,$$
$$\frac{|(A_S^{-})_{yzx}|/N_S}{|A_B^{-}|/N_B} = 8.1, \tag{40}$$

where the values of $A_B^{\pm}$, $(A_S^{+})_{zyx}$ and $(A_S^{-})_{yzx}$ are given in table 1, and $N_S = 10^{18}\,\mathrm{m}^{-2}$ and $N_B = 4.2 \times 10^{26}\,\mathrm{m}^{-3}$ are number densities of BN molecules in a surface monolayer and in the bulk solution, respectively.[2] The value of N_S was calculated from the known fractional coverage of $\gtrsim 0.9$ for BN on water [34] with each BN molecule occupying an area of $\sim 90\,\text{Å}^2$. The ratios being larger than 1 indicates that the orientational ordering of BN molecules on the water surface enhances the chiral response.

We can gain a better understanding of the chiral SFG response from a BN monolayer using the coupled oscillator model. From equations (37), (38), and (39) we find

$$(A_S^{+})_{yzx} = 0, \tag{41}$$

$$(A_S^{-})_{yzx} = \frac{N_S L_S}{2\epsilon_0 \hbar^2} \sum_n \left[\frac{\{\langle g|\mu_{y'}|e_{1_-}\rangle\langle n|\mu_{x'}|g\rangle - \langle g|\mu_{x'}|e_{1_-}\rangle\langle n|\mu_{y'}|g\rangle\}\langle e_{1_-}|\mu_{z'}|n\rangle}{(\omega_2 - \omega_{ng})} + \right.$$
$$\left. + \frac{\{\langle g|\mu_{y'}|e_{1_-}\rangle\langle e_{1_-}|\mu_{x'}|n\rangle - \langle g|\mu_{x'}|e_{1_-}\rangle\langle e_{1_-}|\mu_{y'}|n\rangle\}\langle n|\mu_{z'}|g\rangle}{(\omega_1 - \omega_{ng})} \right], \tag{42}$$

$$(A_S^{+})_{zyx} = \frac{N_S L_S}{2\epsilon_0 \hbar^2} \sum_n \left[\frac{\langle g|\mu_{z'}|e_{1_+}\rangle\{\langle e_{1_+}|\mu_{y'}|n\rangle\langle n|\mu_{x'}|g\rangle - \langle e_{1_+}|\mu_{x'}|n\rangle\langle n|\mu_{y'}|g\rangle\}(\omega_1 - \omega_2)}{(\omega_1 - \omega_{ng})(\omega_2 - \omega_{ng})} \right], \tag{43}$$

$$(A_S^{-})_{zyx} = 0, \tag{44}$$

where L_S is the local-field correction factor for surface. From equations (23), (24), and (43), recalling that only the z' component of $\langle g|\vec{\mu}|e_{1_+}\rangle$ is non-vanishing, we immediately obtain

$$\left|(A_S^{+})_{zyx}/A_B^{+}\right|(N_B/N_S) = 3L_S/L_B, \tag{45}$$

where L_B is the local-field correction factor for bulk. The expression for $|(A_S^{-})_{yzx}/A_B^{-}|(N_B/N_S)$ is more complex. If we neglect contributions from excited states other than $|e_{1_\pm}\rangle$ in equations (24) and (42), we find, from equations (23), (24), and (42),

$$|(A_S^{-})_{yzx}/A_B^{-}|(N_B/N_S) = 3(L_S/L_B)\frac{|\omega_2 - \omega_{e_{1_+}g}|}{|\omega_1 - \omega_2|} \approx 5.6(L_S/L_B), \tag{46}$$

[2] Ref. [16] used $N_S = 2.0 \times 10^{18}\,\mathrm{m}^{-2}$, but the value $N_S = 10^{18}\,\mathrm{m}^{-2}$ appears to be more accurate. This change does not affect the conclusions of [16].

where we took $\omega_1 = 20\,200\,\mathrm{cm}^{-1}$ ($\leftrightarrow$495 nm), $\omega_2 = 9400\,\mathrm{cm}^{-1}$ ($\leftrightarrow$1.064 μm), and $\omega_{e_{1+}g} = 29\,600\,\mathrm{cm}^{-1}$ ($\leftrightarrow$338 nm). It is difficult to calculate the correct local field correction factors for solute molecules in a solution [31]. However, assuming the ratio of (L_S/L_B) is not too different from unity, we conclude that equations (45) and (46) qualitatively explain the observed enhancement of the chiral signal from an oriented surface of BN. Note that, while equation (45) is exact (providing that all BN molecules on the water surface are oriented with their C_2-symmetry axis along the surface normal), equation (46) is obtained assuming a three-level model for BN and therefore it gives a less accurate estimate of the peak enhancement.

Using equations (9) and (37), we can calculate the spectra of $|(\chi_S^{(2)})_{yzx}|^2$, for three different molecular orientations of the BN monomer with the x', y' and z' axes, respectively, along the surface normal, neglecting the contributions from states other than $|e_{1_\pm}\rangle$. The results are shown in figure 13(a). Only the spectrum of $|(\chi_S^{(2)})_{yzx}|^2$ with z' along the surface normal is in qualitative agreement with the experimental spectrum in figure 13(b), deduced from SPP measurements. This confirms the finding that the BN molecules on water are oriented with their C_2-symmetry axis along the surface normal.

Overall, we have demonstrated here that for twisted dimers like BN, the simple coupled-oscillator model can be used to describe the chiral SFG response fairly well. For other types of chiral molecules, models developed to explain linear optical activity presumably can also be extended to explain their chiral SFG response. In the case of molecules with a chiral centre, the calculation for linear optical activity has recently been extended successfully to explain chiral SFG observed in solutions of amino acids [63].

We note in passing that we have so far considered only the deduction of the chiral non-linear susceptibility elements from measurements with selective polarization combinations SPP, PSP, and PPS. Only the chiral elements contribute to the SF signal in these polarization combinations. Since the SF signal is proportional to the square of the absolute value of effective susceptibility, see equations (5) and (6), such measurements cannot distinguish R- and S-enantiomers although the chiral elements for the two enantiomers have opposite signs. To be able to distinguish the two enantiomers, we must introduce some contribution from achiral non-linear susceptibility elements to interfere with the contribution from chiral elements in SFG. The interference of the response from achiral and chiral non-linear susceptibility elements, positive or negative, can then be used to distinguish R- and S-enantiomers. This will be discussed in more detail in the case of chiral SF vibrational spectroscopy in the next section. Fisher *et al.* recently used a dc-field-induced achiral non-linear susceptibility to interfere with the chiral susceptibility and were able to observe distinguishable chiral SFG responses from BN solutions with different enantiomers [64].

5. Chiral sum-frequency spectroscopy of vibrational transitions

With tunable infrared sources, SFG can be used as a spectroscopic tool to probe molecular chirality in vibrational modes associated with selected groups within a chiral molecule. Since vibrational modes are directly related to the molecular structure,

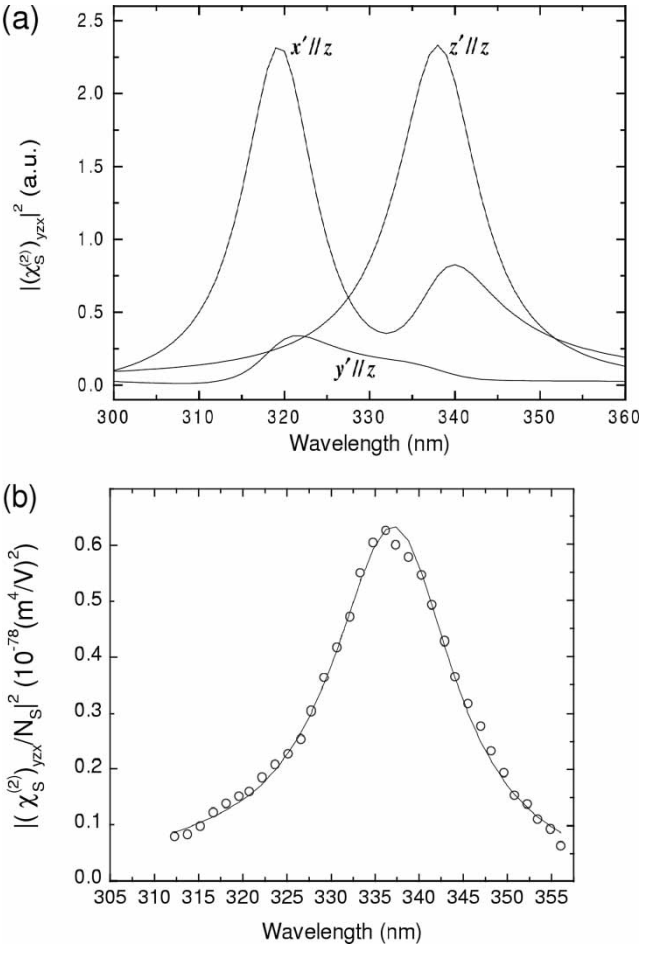

Figure 13. (a) Model prediction for $|(\chi_S^{(2)})_{yzx}(\omega_s)|^2$ for a chiral BN monolayer on water oriented with the molecular axis x', y', or z' along the surface normal. (b) The spectrum of $|(\chi_S^{(2)})_{yzx}/N_S|^2$ of a monolayer of S-BN on water deduced from experiment. The solid curve is the fit from equation (39). Reprinted with permission from [16]. Copyright (2002) by the American Physical Society.

such measurements are expected to be more informative about the chiral structure of molecules. We have demonstrated the possibility in a number of chiral liquids [14].

In our experiment (figure 14(a)), the two input beams, one (ω_1) fixed at 0.532 μm and the other (ω_2) tunable in the infrared between 3.6 and 3.2 μm (2800–3100 cm^{-1}), were both generated by a mode-locked Nd:YAG laser/optical parametric system, with pulse energies of 800 μJ and 200 μJ, respectively. Both had a pulse-width of ~25 ps and a repetition rate of 10 Hz. The two beams overlapped at 90° over an area of 10^{-3} cm^2 on a sample. The samples we studied were chiral liquids in a cell ~1 mm thick, which was much larger than the coherent length l_c, but small enough so that the effect of optical rotation in the sample could be neglected. To avoid the effect of infrared absorption at ω_2, the input beams were overlapped at the entrance surface of the sample.

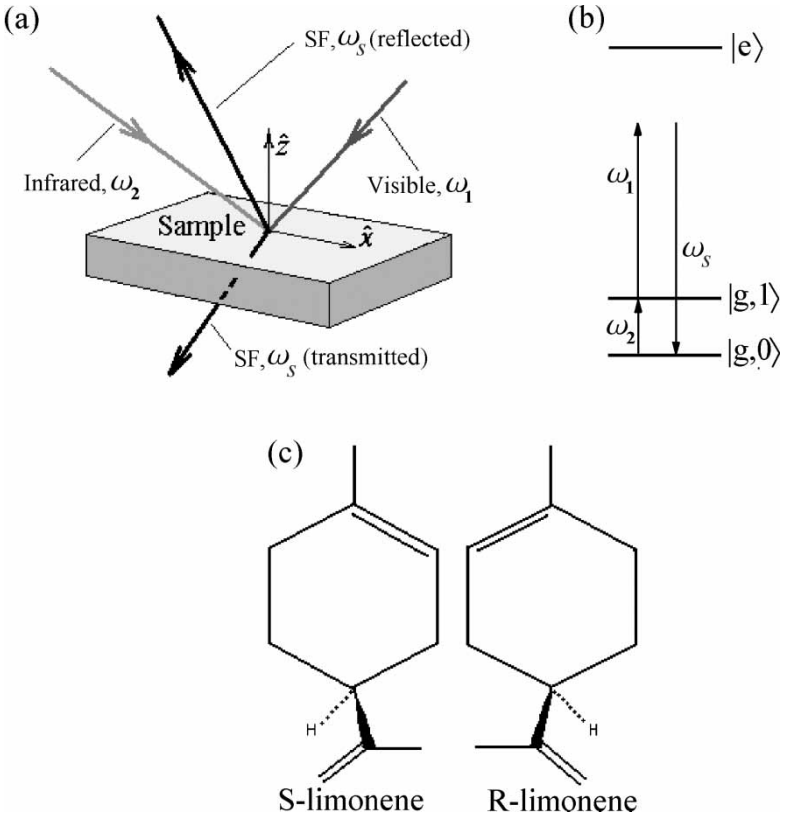

Figure 14. (a) Experimental setup for SF spectroscopy on vibrational transitions. (b) Energy diagram for IR-Visible SFG. (c) Molecular structure of S- and R-limonene

As ω_2 scans over the vibrational resonances of the sample (schematically shown in figure 14(b)), the non-linear susceptibility $\overleftrightarrow{\chi}^{(2)}$ should experience resonant enhancement described by

$$\chi^{(2)}_{ijk}(\omega_2) = (\chi^{(2)}_{NR})_{ijk} + \sum_q \frac{A_{q,ijk}}{\omega_2 - \omega_q + i\Gamma_q} \tag{47}$$

where $(\chi^{(2)}_{NR})_{ijk}$ is a non-resonant contribution, and $A_{q,ijk}$, ω_q, and Γ_q are the amplitude, resonant frequency, and damping constant for the qth vibrational mode. As shown in equation (5), the SF output is proportional to $|\chi^{(2)}_{\text{eff}}|^2$ which depends on $\overleftrightarrow{\chi}^{(2)}$. Recording the SF output as a function of ω_2 yields the SF vibrational spectrum (SFVS).

We have obtained chiral SFVS from chiral liquids in the transmission geometry. Here, we focus the discussion on limonene (chemical formula $C_{10}H_{16}$ depicted in figure 14(c)). Figure 15 displays the SFG spectra (normalized against quartz) in the CH stretch region for the two enantiomers of limonene and their racemic mixture obtained with SPP, PSP, SSP, PPP, and SPS polarization combinations. As mentioned

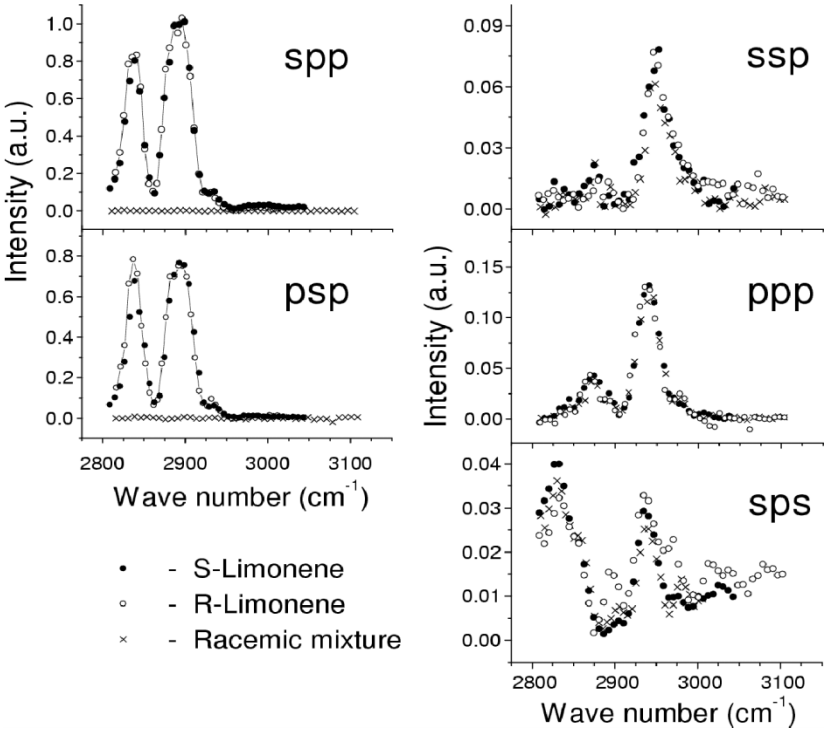

Figure 15. IR–Vis SFG spectra of limonene samples in transmission in SPP, PSP (chiral spectra), SSP, PPP, and SPS (achiral spectra) polarization combinations. Reprinted with permission from [14]. Copyright (2000) by the American Physical Society.

earlier, the SSP, PPP, and SPS spectra involve only the achiral elements of $\overleftrightarrow{\chi}^{(2)}$, whereas the SPP and PSP spectra involve only the chiral elements. The two sets of spectra are clearly very different, indicating that the vibrational modes with strong chirality are not necessarily the dominant modes in the achiral spectra.

The spectra in figure 15 provide the following information.

1. As expected, the achiral SFG spectra for the two limonene enantiomers and the racemic mixture are the same. The chiral SFG spectra for the two enantiomers are also identical, but disappear for the racemic mixture.
2. The peaks in the chiral spectra are $\sim$25 times stronger than those in the achiral SPS spectrum.
3. The chiral spectra yield a spectrum of $|\chi^{\text{bulk}}_{\text{chiral}}(\omega_2)/N_B|^2$ (with $N_B = 3.7 \times 10^{27}\,\text{m}^{-3}$), displayed in figure 16. Fitting of the spectrum using equation (47) allows us to deduce the characteristic parameters for each vibrational mode. They are listed in table 2. The observed resonances can be assigned to [65]: symmetric CH_2 stretch at 2839cm^{-1}, symmetric CH_3 stretch at $2879\,\text{cm}^{-1}$, CH stretch at 2905cm^{-1}, antisymmetric CH_2 stretch at $2936\,\text{cm}^{-1}$, and a very weak symmetric stretch of the C=C double bonded CH_2 group at $2990\,\text{cm}^{-1}$ (not shown in the table).

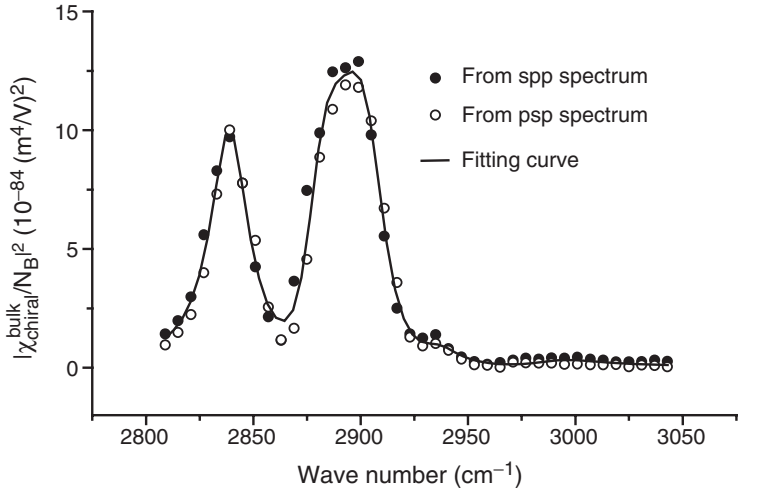

Figure 16. Measured spectral dependence of $|\chi^{bulk}_{chiral}/N_B|^2$ of limonene.

Table 2. Fitting parameters for $\chi^{bulk}_{chiral}(\omega_2)$ of limonene, as described in equation (47). The values of $|(\alpha_{chiral})_q|$ were deduced using equations (12) and (47). Reprinted with permission from [14]. Copyright (2000) by the American Physical Society.

q	A_q (m V^{-1} s^{-1})	$\omega_q/2\pi c$ (cm^{-1})	$\Gamma_q/2\pi c$ (cm^{-1})	$\lvert(\alpha_{chiral})_q\rvert$ (m^3 C V^{-2})
CH_2^{sym}	0.025	2839	11	1.3×10^{-53}
CH_3^{sym}	0.021	2879	12	1.0×10^{-53}
CH	−0.030	2905	13	1.3×10^{-53}
CH_2^{asym}	0.004	2936	11	0.2×10^{-53}

4. Using equations (12) and (47) with $l_B(\omega_s)l_B(\omega_1)l_B(\omega_2) \approx 2.2$ for limonene liquid, we deduced the values of $|\alpha_{chiral}|$ for different modes at resonance and listed them in table 2. They are approximately three orders of magnitude smaller than the typical resonant value of $\sim 2 \times 10^{-50}$ m^3 C V^{-2} of an achiral element of $\vec{\vec{\alpha}}^{(2)}$ for a CH_x stretch vibration (estimated from [30] assuming $\Gamma = 10\,\text{cm}^{-1}$).

As a chiral response, χ^{bulk}_{chiral} has opposite signs for the two enantiomers, but the experiment with SPP, PSP and PPS polarization combinations yielding $|\chi^{bulk}_{chiral}|^2$ cannot distinguish the two. This can, however, be changed by using a PMP polarization combination, where M ('mixed') refers to a linear polarization of the visible input at $\pm 45^\circ$ from its plane of incidence. We then have, from equation (6),

$$(\chi^{(2)}_{eff})_{\pm} = \frac{1}{\sqrt{2}}\left[(\chi^{(2)}_{eff})_{PSP} \pm (\chi^{(2)}_{eff})_{PPP}\right]. \tag{48}$$

The SF output proportional to $|(\chi^{(2)}_{eff})_{\pm}|^2$ will display interference between $(\chi^{(2)}_{eff})_{PSP}$ (chiral) and $(\chi^{(2)}_{eff})_{PPP}$ (achiral) contributions, and the spectra of $|(\chi^{(2)}_{eff})_{+}|^2$ and

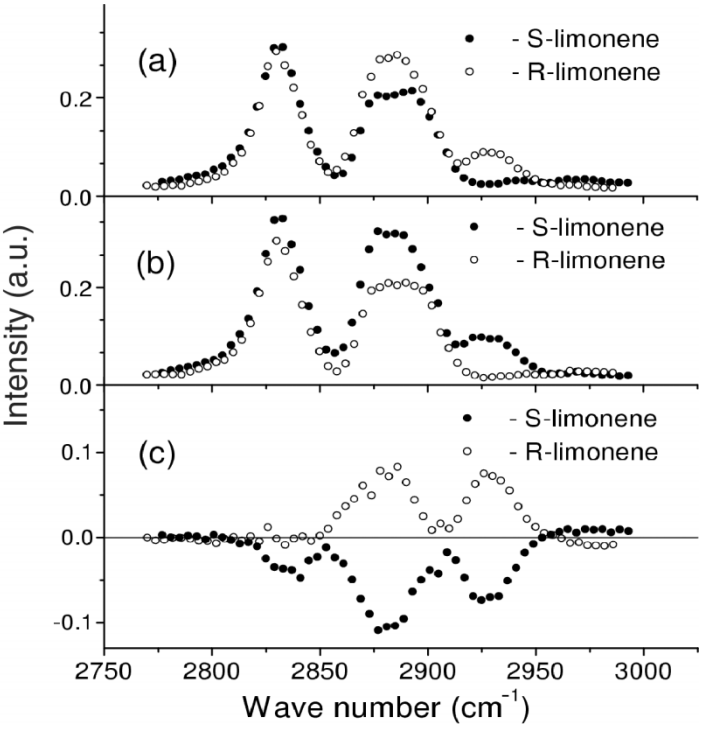

Figure 17. Spectra of S- and R-limonene in mixed polarization combinations: (a) $|(\chi^{(2)}_{\text{eff}})_+|^2$, (b) $|(\chi^{(2)}_{\text{eff}})_-|^2$, and (c) $|(\chi^{(2)}_{\text{eff}})_+|^2 - |(\chi^{(2)}_{\text{eff}})_-|^2$. Reprinted with permission from [14]. Copyright (2000) by the American Physical Society.

$|(\chi^{(2)}_{\text{eff}})_-|^2$ will be different. This is shown in figure 17(a) and (b). If we take the difference of the two spectra, then with

$$\left|\left(\chi^{(2)}_{\text{eff}}\right)_+\right|^2 - \left|\left(\chi^{(2)}_{\text{eff}}\right)_-\right|^2 = \left(\chi^{(2)}_{\text{eff}}\right)_{\text{PSP}}\left(\chi^{(2)}_{\text{eff}}\right)^*_{\text{PPP}} + \left(\chi^{(2)}_{\text{eff}}\right)^*_{\text{PSP}}\left(\chi^{(2)}_{\text{eff}}\right)_{\text{PPP}} \tag{49}$$

the difference spectrum must be inverted when the enantiomer is switched from R to S or vice versa, following the sign switch of the chiral $(\chi^{(2)}_{\text{eff}})_{\text{PSP}}$. This is seen in figure 17(c). Thus the PMP polarization combinations in SFG allow us to distinguish R- and S-enantiomers. However, we note that the difference spectra are now proportional to the product of the chiral $(\chi^{(2)}_{\text{eff}})_{\text{PSP}}$ and achiral $(\chi^{(2)}_{\text{eff}})_{\text{PPP}}$.

We also found experimentally that chiral SFG in reflection from the limonene was below noise. In our experiment, SFG in transmission had a coherent length 20 times larger than SFG in reflection. The result indicates that the chiral SFG in transmission originated from the bulk and contributions from the chiral surface non-linear susceptibility were negligible. The latter must have a value smaller than $5 \times 10^{-22}\,\text{m}^2\,\text{V}^{-1}$. For comparison, a typical value of the achiral surface non-linear susceptibility for SFG in the CH stretch range is $\sim(1-5) \times 10^{-21}\,\text{m}^2\,\text{V}^{-1}$.

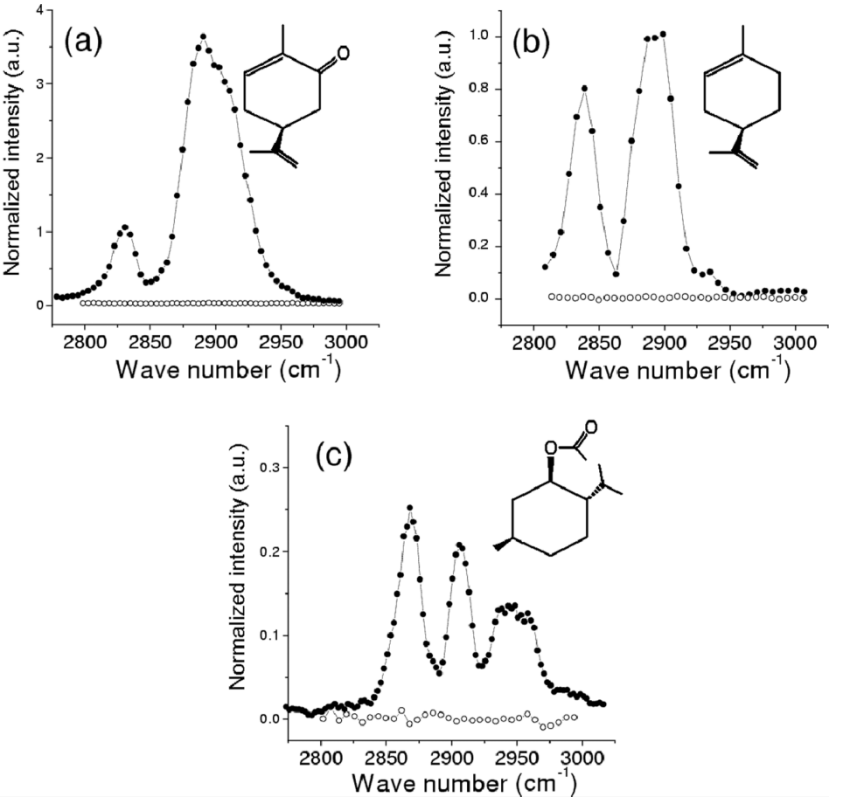

Figure 18. Transmission SFG spectra of different chiral liquids taken in the C–H stretch range with the SPP polarization combination. (a) Carvone, (b) limonene, (c) menthyl acetate. Filled circles are from enantiomeric liquids, and open circles from racemic mixtures.

We have obtained similar SFVS results from carvone (chemical formula $C_{10}H_{14}O$) and menthyl acetate (chemical formula $C_{12}H_{22}O_2$). Figure 18 displays their molecular structures and SFVS in the CH stretch region in comparison with that of limonene obtained with SPP polarization combination in transmission. No SPP spectra were observed from racemic mixtures of all these liquids. The maximum value of $|\chi^{\text{bulk}}_{\text{chiral}}|$ measured from carvone liquid is approximately twice that of limonene, and the maximum value of $|\chi^{\text{bulk}}_{\text{chiral}}|$ measured from menthyl acetate liquid is approximately two times smaller than that of limonene. Similar to limonene, no chiral SF signal was detected in reflection from carvone and menthyl acetate.

To understand why $|\chi^{\text{bulk}}_{\text{chiral}}|/N_B$ is much smaller than expected for electric-dipole allowed elements, we must go to the microscopic description [66]. The crude explanation is as follows. It is seen from figure 14(b) that SFG with a vibrational resonance can be considered as an infrared excitation of the vibrational transition followed by an anti-Stokes Raman transition, i.e.

$$\alpha^{(2)}_{ijk} \propto M_{ij}\mu_k \tag{50}$$

where $\vec{\mu}$ and $\overleftrightarrow{M}$ denote the infrared and anti-Stokes Raman matrix elements. From equations (12) and (13) it then follows that $\chi^{\text{bulk}}_{\text{chiral}}$ is proportional to the antisymmetric part of M_{ij}. It is known that for non-magnetic materials, the antisymmetric Raman scattering is vanishingly small far away from electronic resonance [67]. This then makes $\chi^{\text{bulk}}_{\text{chiral}}$ also small. In addition, the vibrational modes may be associated with groups of atoms that are not chiral by themselves, but become chiral only because they are situated in a chiral molecular structure. The induced chirality in the vibrational modes is expected to be small.

More rigorously, we can obtain from equation (19) the microscopic expression for the non-linear polarizability near a vibrational resonance

$$\alpha^{(2)}_{ijk}(\omega_2) = \frac{1}{\hbar} M_{ij}(\omega_s) \times \frac{\langle g,1|\mu_k|g,0\rangle}{(\omega_2 - \omega_{(g,1)(g,0)} + i\Gamma_{(g,1)(g,0)})}, \tag{51}$$

with the anti-Stokes Raman tensor given by

$$M_{ij}(\omega) = \frac{1}{\hbar}\sum_{n,\delta}\left[\frac{\langle g,0|\mu_i|n,\delta\rangle\langle n,\delta|\mu_j|g,1\rangle}{(\omega - \omega_{(n,\delta)(g,0)} + i\Gamma_{(n,\delta)(g,0)})} - \frac{\langle g,0|\mu_j|n,\delta\rangle\langle n,\delta|\mu_i|g,1\rangle}{(\omega - \omega_{(g,1)(n,\delta)} + i\Gamma_{(g,1)(n,\delta)})}\right]. \tag{52}$$

Here, $|n,\delta\rangle$ denotes a vibronic state where n labels the electronic excitation and δ the vibrational excitation, ω_s is the sum frequency, and $\omega_{(n,\delta)(g,\nu)}$ and $\Gamma_{(n,\delta)(g,\nu)}$ are the transition frequency and damping constant for transition from state $|n,\delta\rangle$ to state $|g,\nu\rangle$, respectively. We assume all molecules are initially in state $|g,0\rangle$.

From equations (12), (13), and (51), the corresponding resonant $\chi^{\text{bulk}}_{\text{chiral}}(\omega_2)$ can be written as

$$\left(\chi^{\text{bulk}}_{\text{chiral}}\right)_R(\omega_2) = \frac{1}{\epsilon_0}\frac{N_B l_B(\omega_s) l_B(\omega_1) l_B(\omega_2)}{6\hbar}\frac{\langle g,1|\vec{\mu}|g,0\rangle}{(\omega_2 - \omega_{(g,1)(g,0)} + i\Gamma_{(g,1)(g,0)})} \cdot \vec{M}^A(\omega_s), \tag{53}$$

with

$$\vec{M}^A(\omega) = \frac{1}{\hbar}\sum_{n,\delta}\left[\frac{\langle g,0|\vec{\mu}|n,\delta\rangle \times \langle n,\delta|\vec{\mu}|g,1\rangle}{(\omega - \omega_{(n,\delta)(g,0)} + i\Gamma_{(n,\delta)(g,0)})} + \frac{\langle g,0|\vec{\mu}|n,\delta\rangle \times \langle n,\delta|\vec{\mu}|g,1\rangle}{(\omega - \omega_{(g,1)(n,\delta)} + i\Gamma_{(g,1)(n,\delta)})}\right]. \tag{54}$$

Note that $[M^A(\omega)]_k = e_{kij}M_{ij}(\omega)$ is a pseudovector.

To see how $\vec{M}^A(\omega)$ diminishes away from electronic resonance, we evaluate the expression for $\vec{M}^A(\omega)$ more explicitly. For perturbation calculation to the first order of electron-vibration coupling, we need to use the Born–Oppenheimer (BO) adiabatic approximation (defined in [68, 69]) plus the first-order non-adiabatic correction [69]. The two contributions have similar magnitudes and tend to cancel each other. Liu and Buckingham [67] and [70] used a similar approach to show

that $\vec{M}^A(\omega)$ is orders of magnitude smaller than its symmetric counterpart. We have carried out a derivation that shows a somewhat different result but the same qualitative conclusion [66]. Here, we sketch briefly our derivation. The details can be found in [66].

Let $H = T_E + T_N + V(q, Q)$ be the molecular Hamiltonian with $|n, \delta\rangle$ and $E_{n,\delta}$ denoting the eigenstates and eigenenergies, where T_E is the electron kinetic energy operator, T_N is the nuclear kinetic energy operator, and $V(q, Q)$ is the potential energy with q being the electronic coordinate, and Q the nuclear coordinate with $Q = 0$ referring to the equilibrium nuclear position of the ground state. In the BO adiabatic approximation [68, 69], one takes $|n, \delta\rangle \approx |n)|\delta_n\rangle$ and $(s|T_N|n) = T_N\delta_{sn}$, where δ_{sn} is Kronecker's delta. We then find, with $V_{sn} \equiv \langle s|(\partial V/\partial Q)_{Q=0}|n\rangle$,

$$|n) \approx |n\rangle + \sum_{s\neq n} |s\rangle \frac{V_{sn}}{E_n^0 - E_s^0} Q. \tag{55}$$

where E_n^0 is the energy of the $|n\rangle$ electronic state obtained from $[T_E + V(q, 0)]|n\rangle = E_n^0|n\rangle$. We define $E_{n,\delta} \approx E_{n,\delta}^{BO} \equiv E_n^0 + \epsilon_{n,\delta}$ as the eigenenergy of $|n)|\delta_n\rangle$ with $\epsilon_{n,\delta}$ being the vibrational energy of the $|\delta_n\rangle$ state obtained from $[T_N + (n|T_E + V(q, Q)|n) - E_n^0]|\delta_n\rangle \equiv H_n^{\text{vib}}|\delta_n\rangle = \epsilon_{n,\delta}|\delta_n\rangle$. In the non-adiabatic correction, $(s|T_N|n)$ is no longer taken as zero for $s \neq n$, but taken as a perturbation to the first order of Q. The BO adiabatic state combined with the non-adiabatic correction then yields [69, 71, 72]

$$|n, \delta\rangle = |n\rangle|\delta_n\rangle + \sum_{s\neq n} |s\rangle \sum_{\nu_s} |\nu_s\rangle \frac{V_{sn}}{\hbar\omega_{(n,\delta)(s,\nu)}} \langle\nu_s|Q|\delta_n\rangle. \tag{56}$$

For simplicity, we shall neglect the vibronic coupling (i.e. the term proportional to V_{sn} in equation (56)) in the ground electronic state and assume $|g, \delta\rangle = |g\rangle|\delta_g\rangle$ because typically the energy separation between ground and excited states is much larger than that between excited states, and thus the contribution of vibronic coupling in the excited states is much more important, as seen in equation (56). We also assume that the Franck–Condon shifts between different electronic states are small so that $\langle 1_s|1_n\rangle \approx \langle 0_s|0_n\rangle \approx 1$ and $\langle 0_g|1_n\rangle = -\langle 0_n|1_g\rangle \ll 1$. Now inserting the wavefunctions of equation (56) into equation (52), keeping terms to the first order in the vibronic coupling, and assuming all wavefunctions real, we obtain for the Raman tensor [69],

$$M_{ij} = M_{ij}^s + M_{ij}^{a/s}, \tag{57}$$

$$M_{ij}^s \equiv \frac{1}{2}(M_{ij} + M_{ji}) = A_{ij} + B_{ij}^s, \tag{58}$$

$$M_{ij}^{a/s} \equiv \frac{1}{2}(M_{ij} - M_{ji}) = B_{ij}^{a/s}, \tag{59}$$

where the superscripts s and a/s denote symmetric and antisymmetric component of the quantity, and

$$A_{ij} = \frac{1}{\hbar}\sum_{n\neq g}\frac{\mu_i^{ng}\mu_j^{ng}\omega_{(n,1)(n,0)}\langle 0_g|1_n\rangle}{(\omega-\omega_{(n,0)(g,0)}+i\Gamma_{(n,0)(g,0)})(\omega-\omega_{(n,1)(g,0)}+i\Gamma_{(n,1)(g,0)})}, \tag{60}$$

$$\begin{aligned} B_{ij}^{s} = {} & \frac{1}{2\hbar^2}\sum_{n\neq g}\sum_{s<n,\neq g} V_{sn}Q_{01} \\ & \times\left(\frac{1}{(\omega-\omega_{(n,1)(g,0)}+i\Gamma_{(n,1)(g,0)})(\omega-\omega_{(s,0)(g,0)}+i\Gamma_{(s,0)(g,0)})}\right. \\ & \left.+\frac{1}{(\omega-\omega_{(n,0)(g,0)}+i\Gamma_{(n,0)(g,0)})(\omega-\omega_{(s,1)(g,0)}+i\Gamma_{(s,1)(g,0)})}\right) \\ & \times(\mu_i^{ng}\mu_j^{sg}+\mu_j^{ng}\mu_i^{sg}), \end{aligned} \tag{61}$$

$$\begin{aligned} B_{ij}^{a/s} = {} & \frac{-1}{2\hbar^2}\sum_{n\neq g}\sum_{s<n,\neq g} V_{sn}Q_{01} \\ & \times\left(\frac{1}{(\omega-\omega_{(n,1)(g,0)}+i\Gamma_{(n,1)(g,0)})(\omega-\omega_{(s,0)(g,0)}+i\Gamma_{(s,0)(g,0)})}\right. \\ & \left.-\frac{1}{(\omega-\omega_{(n,0)(g,0)}+i\Gamma_{(n,0)(g,0)})(\omega-\omega_{(s,1)(g,0)}+i\Gamma_{(s,1)(g,0)})}\right) \\ & \times(\mu_i^{ng}\mu_j^{sg}-\mu_j^{ng}\mu_i^{sg}). \end{aligned} \tag{62}$$

Here we denote $\langle n|\mu_i|g\rangle$ as μ_i^{ng}.

From equations (60)–(62), we see that if ω is off-resonance such that the vibrational frequencies in the denominators are negligible, then the antisymmetric part of the Raman tensor vanishes, but the symmetric part does not. The antisymmetric part becomes more significant as ω approaches molecular electronic resonances.

To have some feeling for the frequency dependence of A_{ij}, B_{ij}^{s}, and $B_{ij}^{a/s}$ on ω, we plot these quantities versus ω in figure 19 assuming a system of only three electronic levels g, n and s with $\mu_i^{ng}\mu_j^{ng} \approx \frac{1}{2}(\mu_i^{ng}\mu_j^{sg}-\mu_j^{ng}\mu_i^{sg}) \approx \frac{1}{2}(\mu_i^{ng}\mu_j^{sg}-\mu_j^{ng}\mu_i^{sg})$, the values of all damping constants being the same for all transitions and taking $\omega_{(n,0)(g,0)} = 50\,000\,\mathrm{cm}^{-1}$ ($\hbar\omega_{(n,0)(g,0)} \approx 6.2\,\mathrm{eV}$), $\omega_{(s,0)(n,0)} = 10\,000\,\mathrm{cm}^{-1}$ ($\hbar\omega_{(s,0)(n,0)} \approx 1.2\,\mathrm{eV}$), $\omega_{(s,0)(g,0)} = 60\,000\,\mathrm{cm}^{-1}$ ($\hbar\omega_{(s,0)(g,0)} \approx 7.4\,\mathrm{eV}$), $\omega_{(s,1)(s,0)} \approx \omega_{(n,1)(n,0)} \approx \omega_{(g,1)(g,0)} = \Omega = 1000\,\mathrm{cm}^{-1}$, and $\Gamma = 500\,\mathrm{cm}^{-1}$. It is seen that the antisymmetric part has a much stronger resonant enhancement toward the electronic resonances than the symmetric parts. On resonance, with $\omega = \omega_{(n,0)(g,0)}$, we have $|B_{ij}^{s}| \sim |B_{ij}^{a/s}|$ and from equations (60)–(62),

$$|M_{ij}^{a/s}/M_{ij}^{s}| \approx |B_{ij}^{a/s}/(A_{ij}+B_{ij}^{s})| \approx |B_{ij}^{a/s}/A_{ij}| \approx \left|\frac{\omega_{(n,1)(n,0)}}{\omega_{(s,1)(n,0)}}\right| \approx \left|\frac{\Omega}{\omega_{(s,0)(n,0)}}\right|. \tag{63}$$

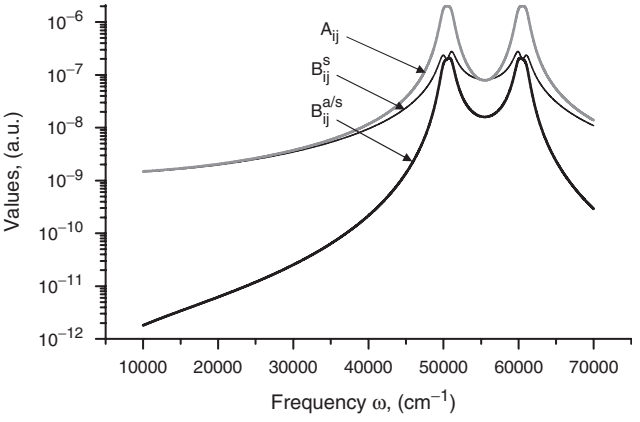

Figure 19. Frequency dependence of the elements of $\overleftrightarrow{A}$, $\overleftrightarrow{B}^{s}$, and $\overleftrightarrow{B}^{a/s}$. Reprinted with permission from [66]. Copyright (2004) American Institute of Physics.

Off-resonance, $\overleftrightarrow{B}^{a/s}$ drops off according to

$$|M_{ij}^{a/s}/M_{ij}^{s}| \approx |B_{ij}^{a/s}/A_{ij}| \approx |B_{ij}^{a/s}/B_{ij}^{s}| \approx \left|\frac{\Omega\omega_{(n,0)(s,0)}}{2(\omega-\omega_{(n,0)(g,0)})(\omega-\omega_{(s,0)(g,0)})}\right|. \quad (64)$$

The difference between on-resonance and off-resonance becomes more significant if $\omega_{(s,0)(n,0)}$ is smaller.

As shown in equation (53), the chiral non-linearity of a bulk liquid for vibrationally resonant SFG is proportional to the antisymmetric part of the Raman tensor. Comparing $|\chi^{\text{bulk}}_{\text{chiral}}|/N_B$ with a typical (achiral) non-linear polarizability element, $|\alpha^{(2)}_{\text{achiral}}|$, we have

$$|\chi^{\text{bulk}}_{\text{chiral}}/N_B|/|\alpha^{(2)}_{\text{achiral}}| \sim |M_{ij}^{a/s}/M_{ij}^{s}| \quad (65)$$

For CH stretch modes observed in our chiral SFG studies, the vibrational frequency is $\Omega \approx 3000\,\text{cm}^{-1}$, and the electronic transition frequencies for the sigma-bonds in CH_x are $\omega_{ng} \approx 70\,000\,\text{cm}^{-1}$ ($\hbar\omega_{ng} \approx 8.7\,\text{eV}$) and $\omega_{sg} \approx 85\,000\,\text{cm}^{-1}$ ($\hbar\omega_{ng} \approx 10.5\,\text{eV}$) [73] (the data for ethane was used as an example). With $\omega_s = \omega_1 + \Omega \approx 20\,000\,\text{cm}^{-1}$, we find, following equation (64),

$$|M_{ij}^{a/s}(\omega_s)/M_{ij}^{s}(\omega_s)| \sim 1/150. \quad (66)$$

The value of $|\chi^{\text{bulk}}_{\text{chiral}}|$ is expected to reduce further knowing that the chirality in the CH_x group comes only because it interacts with its chiral environment in the molecular structure. This explains why the observed $|\chi^{\text{bulk}}_{\text{chiral}}/N_B|$ was three orders of magnitude weaker than its achiral counterpart.

We also consider here the chiral elements of surface $\overleftrightarrow{\chi}_S^{(2)}$ for SFVS, although away from electronic resonance, they seem to be too small to be measurable so far. As a good approximation, we assume the symmetric part of the Raman tensor to be dominant. Then, from equations (8), (9), and (50), we have, for an azimuthally isotropic surface with $\vec{z}$ along the surface normal, $(\chi_S^{(2)})_{xyz} = -(\chi_S^{(2)})_{yxz} = 0$, and

$$(\chi_S^{(2)})_{yzx} = -(\chi_S^{(2)})_{xzy} = -(\chi_S^{(2)})_{zxy} = (\chi_S^{(2)})_{zyx} \equiv \chi_{\text{chiral}}^{\text{surface}}. \tag{67}$$

The value of $\chi_{\text{chiral}}^{\text{surface}}$ depends on the specific molecular structure and orientation on the surface. We show here that contrary to the bulk case, the surface chiral response in SFVS is mainly associated with the symmetric part, rather than the antisymmetric part, of the Raman tensor. This has also been noted in [52].

More generally, one can prove that the maximum absolute value of the chiral elements of $\overleftrightarrow{\chi}_S^{(2)}$ per molecule is greater than or equal to the value of $|\chi_{\text{chiral}}^{\text{bulk}}|$ per molecule for both vibrational and electronic SFG spectroscopies (neglecting the local-field corrections). This follows from the fact that for any surface orientational distribution and in any Cartesian laboratory (i, j, k) and molecular (ξ, η, ζ) coordinate systems, we have

$$\begin{aligned} e_{ijk} \sum_{\xi,\eta,\zeta} \alpha_{\xi\eta\zeta}^{(2)} \langle (\hat{i}\cdot\hat{\xi})(\hat{j}\cdot\hat{\eta})(\hat{k}\cdot\hat{\zeta})\rangle &= \sum_{\xi,\eta,\zeta} \alpha_{\xi\eta\zeta}^{(2)} \langle e_{ijk}\xi_i\eta_j\zeta_k\rangle \\ &= \sum_{\xi,\eta,\zeta} \alpha_{\xi\eta\zeta}^{(2)} \langle \hat{\xi}\cdot(\hat{\eta}\times\hat{\zeta})\rangle = e_{ijk}\alpha_{ijk}^{(2)} = 6\alpha_{\text{chiral}} \end{aligned} \tag{68}$$

and then, from equations (8), (9) and (12), neglecting the local-field correction factors, we obtain

$$\frac{1}{3N_S}((\chi_S^{(2)})_{xyz} + (\chi_S^{(2)})_{zxy} + (\chi_S^{(2)})_{yzx}) = \frac{\chi_{\text{chiral}}^{\text{bulk}}}{N_B}. \tag{69}$$

6. Doubly resonant SFG

As discussed in the preceding section, the chiral response from the bulk in SFVS should experience extraordinarily strong resonant enhancement when the sum frequency ω_s approaches an electronic resonance, not only because of the usual resonant enhancement but also because the antisymmetric part of the Raman tensor becomes increasingly significant. This should considerably improve the sensitivity of SF vibrational spectroscopy to probe chirality. To verify the prediction, we have carried out doubly resonant (DR) infrared–ultraviolet (IR–UV) SFG measurements on a solution of 0.46 M BN in acetone.

To have doubly resonant enhancement in IR–UV SFG, the vibrational mode must be coupled to the electronic state in resonance. The two UV absorption peaks for BN

shown in figure 7(b) arise from $\pi \rightarrow \pi^*$ excitations in the naphthalene rings [74]. We expect that the vibrational modes associated with deformation (stretching) of the naphthalene rings of BN in the range of 1300–1600 cm^{-1} [75, 76] should be strongly coupled to these electronic excitations. Therefore, we focus on DR SF spectra of vibrational modes in this range.

In the experiment, we used a UV input (ω_1) tunable from 3.35 to 3.60 eV (370 to 345 nm) and an infrared input (ω_2) tunable from 1300 to 1600 cm^{-1}. Both were generated from a Nd:YAG laser-pumped optical parametric system and had a pulse energy of $\sim$100 μJ and pulse-width $\sim$25 ps. The SF vibrational spectra taken in the reflected direction were obtained by scanning ω_2 over vibrational resonances of BN with ω_1 simultaneously adjusted to keep $\omega_s = \omega_1 + \omega_2$ fixed. The measurements were repeated for different values of ω_s.

Figure 20(a) displays a representative set of sum-frequency vibrational spectra at several sum frequencies obtained from the BN solution using the SPP polarization combination. There is a strong resonant enhancement as ω_s approaches the first excitonic resonance of BN at 337 nm. Selected vibrational peaks in the 335 nm spectrum show an enhancement of more than 10^5 with respect to the off-resonant spectrum at 500 nm. For comparison, we present in figure 20(b) the achiral vibrational spectra of[3] $|(\chi_S^{(2)})_{yyz}/N_S|^2$ for a monolayer of BN on water taken at the same set of ω_s values with the SSP polarization combination. The resonant enhancement (comparing again spectra at 335 and 500 nm) is only about 200. At the peak of the resonance, the achiral element $|(\chi_S^{(2)})_{yyz}/N_S|$ is only 5 times larger than the chiral element $|\chi_{\text{chiral}}^{\text{bulk}}/N_B|$, as expected from the theoretical estimate described in the previous section.

Note that the observed sum-frequency vibrational spectra exhibit very different resonant enhancements for different vibrational modes. This is especially clear in the chiral SF spectra, and is the result of very different vibronic couplings for different modes. Strong resonant enhancement of selective vibrational modes allows better assignment of the vibrational modes. This as well as possible deduction of vibronic couplings from the spectra is known to be the other important advantage of resonant Raman spectroscopy. Doubly resonant chiral modes will certainly help in attempts to understand chiral structure of chiral molecules.

For BN, the chiral responses of the 1375 cm^{-1} and 1430 cm^{-1} vibrational modes exhibit the strongest resonant enhancement near the first electronic resonance. They are shown in figure 21 in comparison with the achiral responses of the same modes. The chiral response decreases much faster than the achiral response as ω_s moves away from resonance. The theoretical curves in figure 21 are calculated using the vibrational frequency $\Omega = 1400\,cm^{-1}$, damping constants $\Gamma = 500\,cm^{-1}$, and two exciton-split electronic excited states at 3.67 and 3.89 eV in equations (61) and (62). The agreement between theory and experiment on resonant dispersion appears fairly good.

Equation (69) suggests that with the very strong enhancement of $|\chi_{\text{chiral}}^{\text{bulk}}/N_B|$ near double resonance we should be able to observe chiral vibrational spectra of a monolayer

[3] Ref. [15] used $N_S = 2.0 \times 10^{18}\,m^{-2}$, but the value $N_S = 10^{18}\,m^{-2}$ appears to be more accurate. This change does not affect the conclusions of [15].

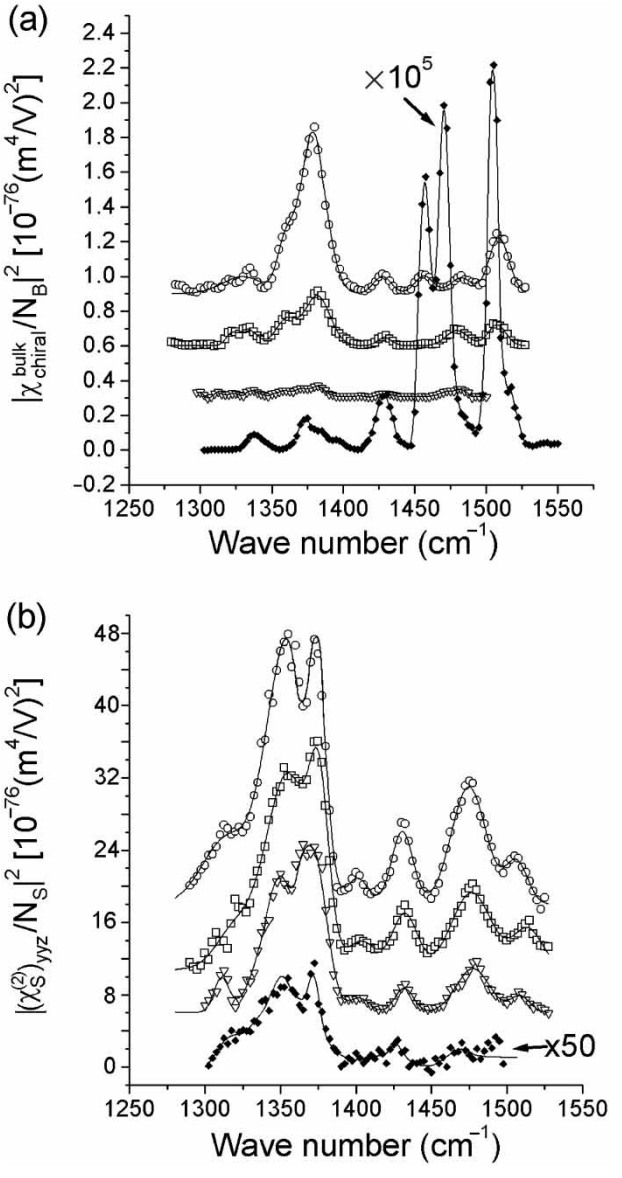

Figure 20. (a) Chiral spectra of $|\chi^{bulk}_{chiral}/N_B|^2$ of a 0.462 M solution of R-BN in acetone and (b) achiral spectra $|(\chi^{(2)}_S)_{yyz}/N_S|^2$ of an R-BN monolayer on water with sum-frequency at 335 nm (open circles), 340 nm (open squares), 345 nm (open down triangles) and ~500 nm (solid diamonds). The 500 nm spectra of $|\chi^{bulk}_{chiral}/N_B|^2$ and $|(\chi^{(2)}_S)_{yyz}/N_S|^2$ were enhanced by 10^5 and 50, respectively. Vertical shifts are used to separate the spectra in the display and lines are to guide the eye.

by SF vibrational spectroscopy. While achiral SF vibrational spectra of molecular monolayers were routinely measured in recent years, the chiral counterparts had never been observed by any techniques. Using doubly resonant SFG on BN on water, we succeeded in recording the first chiral vibrational spectrum of a molecular monolayer.

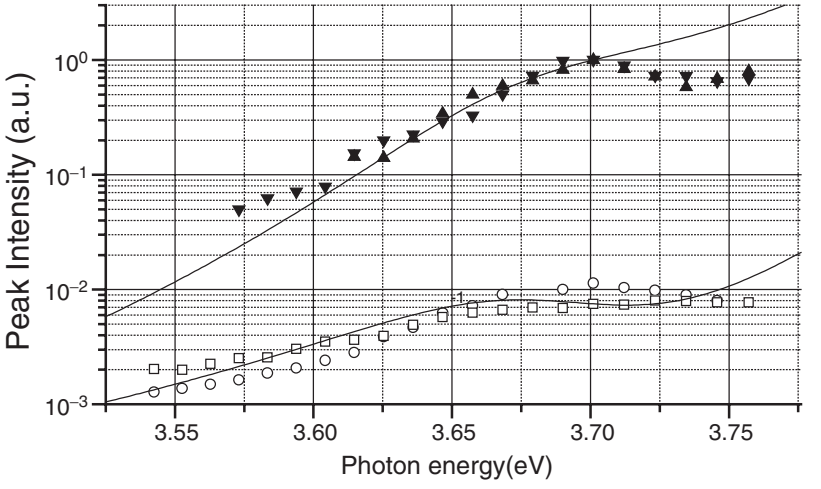

Figure 21. Peak strengths of vibrational modes of BN at 1375 cm^{-1} and 1430 cm^{-1} in $|\chi^{bulk}_{chiral}/N_B|^2$ (solid down and up triangles, respectively) and in $|(\chi^{(2)}_S)_{yyz}/N_S|^2$ (open squares and circles, respectively) versus $\hbar\omega_s$. Solid lines are calculated from the frequency dependence of $|B^{a/s}_{ij}|^2$ (upper curve) and $|B^{s}_{ij}|^2$ (lower curve) in equations (61) and (62). A vertical shift is used to separate the 'chiral' and 'achiral' data sets. Reprinted with permission from [15]. Copyright (2003) by the American Physical Society.

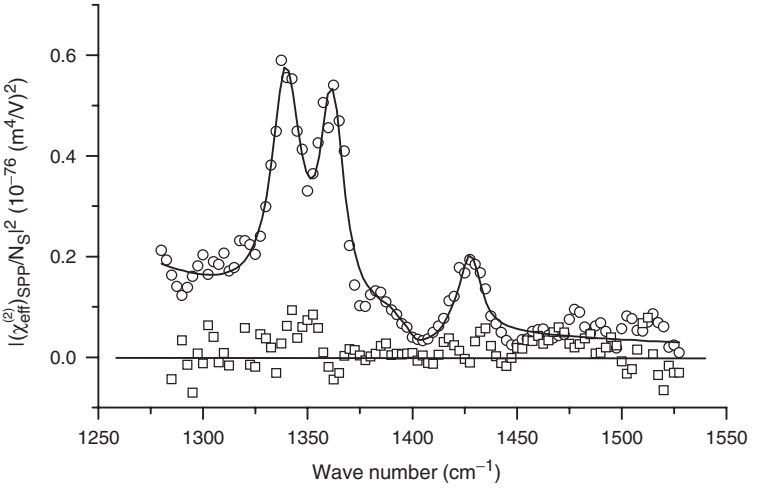

Figure 22. SPP spectra of monolayers of R-BN (circles) and racemic mixture of BN (squares) on water with sum-frequency at 335 nm.

This is seen in figure 22 for a BN monolayer on water. No chiral spectrum could be detected if the R- or S-enantiomer of the monolayer was replaced by a racemic mixture. Because of the orientational order of the BN molecules adsorbed on water, the SPP chiral spectrum appears different from the bulk one. To understand the difference, we need *ab initio* calculations that can relate the spectra to the molecular structure and orientation of BN.

7. Conclusion

Although SFG as an electric-dipole-allowed process in chiral liquids was considered theoretically as early as in 1965 [8], it was not confirmed experimentally until very recently. We now understand that despite its being electric-dipole allowed, the effect is intrinsically weak far away from resonance. Observation of the effect requires resonance enhancement. While this restriction makes chiral liquids not useful as non-linear media for frequency conversion, it does allow the process to probe chirality in electronic and vibrational transitions of chiral molecules. Here we have described the recent progress in developing SFG (and SHG as a special case of SFG) as a spectroscopic tool to study molecular chirality. We have limited our study to isotropic chiral liquids and azimuthally isotropic chiral surface monolayers.

Traditional optical techniques to probe chirality, such as circular dichroism and Raman optical activity, have limited sensitivities because the optical processes are electric-dipole forbidden [4]. They cannot be used reliably to detect chirality from a molecular monolayer or thin film. Being electric-dipole allowed, SFG could be more sensitive and therefore could become a unique spectroscopic technique for studies of chirality of surfaces, monolayers and thin films. Moreover, it is possible to probe exclusively the non-linear chiral response using selective input/output polarization combinations in SFG. This further enhances the sensitivity because unlike linear circular dichroism, it does not require taking the difference of two spectra of nearly equal strengths. Mixing chiral and achiral responses in SFG, R- and S-enantiomers can be distinguished.

We show that SFG as a tool to probe chirality in electronic transitions of molecules can indeed have a monolayer sensitivity. The observed chiral spectra for molecules in an oriented monolayer and in isotropic bulk are generally different because of the different orientational distributions. They can be theoretically fitted by a microscopic expression for the non-linear chiral response if the energy states and corresponding wavefunctions of the molecule are known. This is the case of BN for which a quantum coupled-oscillator model works well. It also shows that different techniques such as SFG and linear circular dichroism probe different aspects of the chiral structure of a molecule. SFG as a tool to probe chirality in vibrational transitions is less sensitive. If the sum frequency is away from electronic resonances, the bulk chiral non-linear susceptibility for SFG is expected to be very small under the Born–Oppenheimer adiabatic approximation with first-order non-adiabatic correction. However, as the sum frequency approaches an electronic resonance, one can expect an unusually strong resonant enhancement of the chiral response because in addition to the usual resonant enhancement, there is also the enhancement due to the increasingly poor cancellation of different terms in the relevant Raman tensor elements. This very strong resonant enhancement then allows probing vibrational chirality of a surface monolayer possible. Double resonance requires coupling of the electronic transition with the vibrational mode. It therefore also helps us in assigning the vibrational modes.

The monolayer sensitivity of chiral SFG provides unique opportunities for *in situ* studies of chiral monolayers and thin films. Another area where it may be advantageous to use chiral SFG spectroscopy instead of CD or ROA is the study of the dynamics of conformational change of chiral molecules under pump excitations. It is known that

CD and ROA spectroscopic techniques measure the difference in the optical responses of the chiral medium for left and right circularly polarized light. Generally, two measurements are required to obtain the information. The relative difference in absorbance or scattering intensity is 10^{-3}–10^{-5} for vibrational CD and ROA and $\sim 10^{-2}$ for electronic CD [5, 6]. Therefore, it is difficult to extract such information with precision in pump-probe experiments for dynamics studies [77, 78], especially for vibrational transitions. Chiral SFG, on the other hand, requires only one measurement to ascertain chirality. The time-resolved chiral SFG spectra in pump-probe experiments are expected to be of the same quality as those presented in this paper.

The high sensitivity and selectivity of SFG as well as its potential for *in situ* time-dependent studies could open many opportunities for research on chirality in chemistry and biology. However, what we have described here is still only the very beginning of an attempt in developing SFG as a novel technique for probing chirality. Much more work in both theory and experiment, especially in relating chiral SF spectra with molecular chiral structures or arrangement, is needed.

Acknowledgements

This work was supported by the Director, Office of Energy Research, Office of Basic Energy Sciences, Materials Science Division of the US Department of Energy under Contract No. DE-AC03-76SF00098.

References

[1] W. Kelvin, *Baltimore Lectures on Molecular Dynamics and the Wave Theory of Light* (C.J. Clay, London, 1904).
[2] P. Ball, *Designing the Molecular World* (Princeton University Press, Princeton, NJ, 1996).
[3] G. Blaschke, H. P. Kraft, K. Fickentscher, and F. Kohler, Arzneim.-Forsch./Drug Res. **29,** 1640 (1979).
[4] L. D. Barron, *Molecular Light Scattering and Optical Activity* (Cambridge University Press, Cambridge, 1982).
[5] L. A. Nafie, Annu. Rev. Phys. Chem. **48,** 357 (1997).
[6] J. Hilario, D. Drapcho, R. Curbelo, and T. A. Keiderling, Appl. Spectr. **55,** 1435 (2001).
[7] L. D. Barron, L. Hecht, E. W. Blanch, and A. F. Bell, Progr. Biophys. Mol. Biol. **73,** 1 (2000).
[8] J. A. Giordmaine, Phys. Rev. **138,** A1599 (1965).
[9] G. Wagnière, J. Chem. Phys. **77,** 2786 (1982).
[10] P. M. Rentzepis, J. A. Giordmaine, and K. W. Wecht, Phys. Rev. Lett. **16,** 792 (1966).
[11] P. Fischer, D. S. Wiersma, R. Righini, B. Champagne and A. D. Buckingham, Phys. Rev. Lett. **85,** 4253 (2000).
[12] M. A. Belkin, S. H. Han, X. Wei, and Y. R. Shen, Phys. Rev. Lett. **87,** 113001 (2001).
[13] T. Petralli-Mallow, T. M. Wong, J. D. Byers, H. I. Yee, and J. M. Hicks, J. Phys. Chem. **97,** 1383 (1993).
[14] M. A. Belkin, T. A. Kulakov, K.-H. Ernst, L. Yan, and Y. R. Shen, Phys. Rev. Lett. **85,** 4474 (2000).
[15] M. A. Belkin and Y. R. Shen, Phys. Rev. Lett. **91,** 213907 (2003).
[16] S. H. Han, N. Ji, M. A. Belkin, and Y. R. Shen, Phys. Rev. B **66,** 165415 (2002).
[17] R. Cameron and G. C. Tabisz, Mol. Phys. **90,** 159 (1997).
[18] H. Mesnil and F. Hache, Phys. Rev. Lett. **85,** 4257 (2000).
[19] H. Mesnil, M. C. Schanne-Klein, F. Hache, M. Alexandre, G. Lemercier, and C. Andraud, Chem. Phys. Lett. **338,** 269 (2001).
[20] A. P. Shkurinov, A. V. Dubrovskii, and N. I. Koroteev, Phys. Rev. Lett. **70,** 1085 (1993).
[21] N. I. Koroteev, Biospectroscopy **1,** 341 (1995).
[22] Y. R. Shen, in *Frontiers in Laser Spectroscopy*, *Proc. Int. School of Physics 'Enrico Fermi', Course CXX*, edited by T. W. Hansch and M. Inguscio (North Holland, Amsterdam, 1994), pp. 139–165.

[23] P. S. Pershan, Phys. Rev. B **130,** 919 (1963).
[24] J. D. Jackson, *Classical Electrodynamics*, 3rd ed. (John Wiley, New York, 1999). In this paper we used the electric-quadrupole moment defined as 1/6 of that in this book.
[25] H. Held, A. I. Lvovsky, X. Wei, and Y. R. Shen, Phys. Rev. B **66,** 205110 (2002).
[26] P. N. Butcher and D. Cotter, *The Elements of Nonlinear Optics* (Cambridge University Press, New York, 1990), pp. 24-27.
[27] M. Born and E. Wolf, *Principles of Optics* (Pergamon Press, New York, 1970).
[28] Y. R. Shen, *The Principles of Nonlinear Optics* (John Wiley, New York, 1984).
[29] X. Zhuang, P. B. Miranda, D. Kim, and Y. R. Shen, Phys. Rev. B **59,** 12632 (1999).
[30] X. Wei, X. W. Zhuang, S. C. Hong, T. Goto, and Y. R. Shen, Phys. Rev. Lett. **82,** 4256 (1999).
[31] F. J. P. Schuurmans, P. de Vries, and A. Lagendijk, Phys. Lett. A **264,** 472 (2000).
[32] H. R. Philipp, in *Handbook of Optical Constants of Solids*, edited by E. D. Palik (Academic Press, New York, 1985), pp. 719–745, and references therein.
[33] S. Singh, in *Handbook of Lasers*, edited by R. J. Pressley (Chemical Rubber Co., Cleveland, Ohio, 1971), p. 489 and p. 497.
[34] J. D. Byers, H. I. Yee, and J. M. Hicks, J. Chem. Phys. **101,** 6233 (1994).
[35] J. D. Byers, H. I. Yee, T. Petralli-Mallow, and J. M. Hicks, Phys. Rev. B **49,** 14643 (1994).
[36] T. Verbiest, M. Kauranen, J. J. Maki, M. N. Teerenstra, A. J. Schouten, R. J. M. Nolte, M. Kauranen, and A. Persoons, J. Chem. Phys **103,** 8297 (1995).
[37] J. M. Hicks, T. Petralli-Mallow, and J. D. Byers, Faraday Discuss. **99,** 341 (1994).
[38] J. M. Hicks and T. Petralli-Mallow, Appl. Phys. B **68,** 589 (1999).
[39] T. P. Petralli-Mallow, A. L. Plant, M. L. Lewis, and J. M. Hicks, Langmuir **16,** 5960 (2000).
[40] M. Kauranen, T. Verbiest, J. Maki, and A. Persoons, J. Chem. Phys. **101,** 8193 (1994).
[41] S. Sioncke, T. Verbiest, and A. Persoons, Mat. Sci. Eng. R **42,** 115 (2003).
[42] S. V. Elshocht, T. Verbiest, M. Kauranen, A. Persoons, B. M. W. Lengeveld-Voss, and E. W. Meijer, J. Chem. Phys. **8201,** 107 (1997).
[43] M. Kauranen, J. J. Maki, T. Verbiest, S. V. Elshocht, and A. Persoons, Phys. Rev. B **1985,** 55 (1997).
[44] S. Cattaneo, E. Vuorimaa, H. Lemmetyinen, and M. Kauranen, J. Chem. Phys. **120,** 9246 (2004).
[45] M. C. Schanne-Klein, F. Hache, A. Roy, C. Flytzanis, and C. Payrastre, J. Chem. Phys. **108,** 9436 (1999).
[46] M. J. Crawford, S. Haslam, J. M. Robert, Y. A. Gruzdkov, and J. G. Frey, Chem. Phys. Lett. **229,** 260 (1994).
[47] M. A. Kriech and J. C. Conboy, J. Am. Chem. Soc. **125,** 1148 (2003).
[48] M. A. Kriech and J. C. Conboy, J. Opt. Soc. Am. B **21,** 1013 (2004).
[49] F. Hache, H. Mesnil, and M. C. Schanne-Klein, Chem. Phys. Lett. **338,** 159 (2001).
[50] M. C. S.-K. T. Boulesteix, F. Hache, M. Alexandre, G. Lemercier, and C. Andraud, Chem. Phys. Lett. **362,** 103 (2002).
[51] F. Hache, T. Boulesteix, M. C. Schanne-Klein, M. Alexandre, G. Lemercier, and C. Andraud, J. Phys. Chem. B **107,** 5261 (2003).
[52] B. J. Burke, A. J. Moad, M. A. Polizzi, and G. J. Simpson, J. Am. Chem. Soc. **125,** 9111 (2003).
[53] M. A. Polizzi, R. M. Plocinik, and G. J. Simpson, J. Am. Chem. Soc. **126,** 5001 (2004).
[54] S. A. Mitchell and R. A. McAloney, J. Phys. Chem. B **108,** 1020 (2004).
[55] S. H. Han, M. A. Belkin, and Y. R. Shen, Opt. Lett. **29,** 1527 (2004).
[56] M. A. Belkin, Y. R. Shen, and C. Flytzanis, Chem. Phys. Lett. **363,** 479 (2002).
[57] I. Hanazaki and H. Akimoto, J. Am. Chem. Soc. **94,** 4102 (1972).
[58] W. Kuhn, Trans. Faraday Soc. **26,** 293 (1930).
[59] F. Hache, H. Mesnil, and M. C. Schanne-Klein, J. Chem. Phys. **115,** 6707 (2001).
[60] L. D. Barron, *Molecular Light Scattering and Optical Activity* (Cambridge University Press, Cambridge, 1982), chapter 5.
[61] A. Rodger and B. Nordén, *Circular Dichroism and Linear Dichroism* (Oxford University Press, Oxford, 1997), chapter 5.
[62] N. Mataga and T. Kubota, *Molecular Interactions and Electronic Spectra* (Marcel Dekker, New York, 1970), chapter 5.
[63] N. Ji and Y. Shen, J. Am. Chem. Soc., **126,** 15008 (2004).
[64] P. Fischer, A. D. Buckingham, K. Beckwitt, D. S. Wiersma, and F. W. Wise, Phys. Rev. Lett. **91,** 173901 (2003).
[65] G. Herzberg, *Molecular Spectra and Molecular Structure* (Krieger, Malaber, FL, 1989–1991).
[66] M. A. Belkin, Y. R. Shen, and R. A. Harris, J. of Chem. Phys. **120,** 10118 (2004).
[67] F. Liu, J. Phys. Chem. **95,** 7180 (1991).
[68] C. J. Ballahausen and A. E. Hansen, Annu. Rev. Phys. Chem. **23,** 15 (1972).
[69] B. B. Johnson and W. L. Peticolas, Annu. Rev. Phys. Chem. **27,** 465 (1976).
[70] F. Liu and A. D. Buckingham, Chem. Phys. Lett. **207,** 325 (1993).

[71] F. Galluzzi, Nuovo Cimento Soc. Ital. Fis. **5D,** 100 (1985).
[72] B. B. Johnson, L. A. Nafie, and W. L. Peticolas, Chem. Phys. **19,** 303 (1977).
[73] E. E. Koch and M. Skibowski, Chem. Phys. Lett. **9,** 429 (1971).
[74] C. N. R. Rao, *Ultraviolet and Visible Spectroscopy. Chemical Applications* (Plenum Press, New York, 1975).
[75] H. A. Szymanski, *Interpreted Infrared Spectra* (Plenum Press, New York, 1967), Vol. 3.
[76] V. Setnička, M. Urbanová, P. Bouř, V. Král, and K. Volka, J. Phys. Chem. A **105,** 8931 (2001).
[77] R. A. Goldbeck, D. B. Kim-Shapiro, and D. S. Kliger, Annu. Rev. Phys. Chem. **48,** 453 (1997).
[78] X. Xie and J. D. Simon, Rev. Sci. Instrum. **60,** 2614 (1989).